

Answers to the second Referee R2.

We want to thank Dr. Frey to review our study and making comments that allow to improve our manuscript.

Legend of styles

- **Reviewer comment**
- Author's answer
- (R2#i): flag to relate the change in the new manuscript (see author's comment)
- *"Change in the manuscript"*

Major comments

Meteorological conditions:

You mention and compare data from four different field campaigns. However, you only very briefly mention the differences in conditions of these campaigns. I think it would be useful to know more about what distinguishes the data sets (see comment above). Like major differences in meteorological or dynamical conditions, land/sea convection or orographical effects, monsoon or other special season, development stages of the MCS during the aircraft observations (developing, mature, decaying), microphysical characteristics as particle shapes which you would get from the optical array probes, or any other conditions that could lead to specific characteristics of the respective datasets.

This study aims to document some of ice microphysical properties (not all) in MCS as function of Z and T. It uses a merged dataset of in-situ measurement performed in 4 MCS over 4 different locations. Main tendencies (median calculation) are calculated as function for this merged dataset. However, it is a will that we take only into account as function of Z and T, as this results could be used in future studies using CloudSat radar reflectivity profiles or the future EarthCare mission's data. In this conditions only T, Z and the locations of the data will be known. This is why, we study the impact of the locations of MCS globally, and not as function of others conditions. We agree that further investigations could be provided taking into account meteorological conditions and dynamics, as life cycle of MCS (developing, mature, and decaying) could also be taken into consideration. This kinds of studies would need more information than these provided by our dataset, to me more accurate and the use of passive remote sensing from geostationary satellites would be helpful for this. This is why we think it is beyond of the topic of this study. It would make it more complex to understand. However, we can provide add some information. The datasets include MCS from West African monsoon that developed over the continent, MCS linked to the ITCZ over the Indian Ocean during the wet MJO phase and the dry MJO phase (small isolated convective systems), MCS developed over land/ocean/cost during the North Australian monsoon and MCS developed over land/ocean/cost during the wet season over the north of south America. Also, MCS were sampled in there mature stage.

We propose to add some comments in the beginning of section 2 (R2#1):

"This study uses a data set where MCSs were observed in four different locations in the tropics and related to two different projects:

- 1. Megha-Tropiques in Niamey, during July and August 2010: observation of continental MCS formed over the region of Niamey (Niger) during the West African Monsoon (Drigeard et al., 2015; Fontaine et al., 2014; Roca et al., 2015). These MCS developed over the continent. 7665 points of 5 seconds.*
- 2. Megha-Tropiques in Maldives, during November and December 2011: observation of oceanic MCS developed over the southern part of the Maldives and related to the ITCZ (Inter Tropical Convergence Zone) in the Indian Ocean. (Fontaine et al., 2014; Martini et al., 2015; Roca et al., 2015). It includes MCS developed during the wet phase of MJO and two event with isolated convective systems developed during the dry phase of MJO. 3347 points of 5 seconds.*

3. HAIC-HIWC in Darwin, from January to March 2014: observations of MCS formed over Darwin and the North-East coast of Australia during the North Australian Monsoon (Leroy et al., 2016; Protat et al., 2016; Strapp et al. 2016; Leroy et al. 2017, Fontaine et al. 2017). During this campaigns, MCS developed over the land, the ocean, and near the coast. 23265 points of 5 seconds.
4. HAIC-HIWC in Cayenne during May 2015: observations of MCS developed over the French Guyana during the peak of its raining season (Yost et al., 2018). Same as for Darwin, MCS developed over the land, the ocean, and near the coast. 21567 points of 5 seconds.

Note that observations were performed in mature MCS.”

Naming convention:

The merged data set from the four campaigns is sometimes named differently in the manuscript and figures (tropical, global, global tropical...). Please keep it to one name! I would suggest not to use 'global' as it only contains tropical campaigns. As it is not clear whether different locations in the tropics have a significant influence on the data, I would suggest simply using 'merged' (or 'combined') data set, that makes it clear that not data from all over the tropics are used (as might be possible in satellite data studies for example).

The comment is taken into account, and a new naming convention will be used for the “tropical dataset” such “merged dataset”.

Radar reflectivity zones:

How were the thresholds for the 8 zones chosen? How do you motivate the thresholds?

Is it possible to interpret each zone in respect to a certain MCS development stage, or do they distinguish in some other MCS characteristic?

In some cases it seems that particularly the lower classes do not really differ from each other (e.g. page 6, line 2/3 or page 25, line 32/33). What is the reason to keep separate zones and not combining them into one?

The description of how were chosen the limits of the 8 MCS reflectivity zones is given in the manuscript page 5 line 5 to line 13.

The motivation to choose limits of MCS reflectivity zones regarding the percentiles given in Figure 1 and Table A1 holds in two facts. First, the variability of Z vary along the altitude. We can observe in Figure 1 that Z extend from about -20dBZ to 18 dBZ at 260K while it spread out from -10dBZ to 10 dBZ at 200K. So, this has to be considered if we want to sort our dataset as function of T and Z. So the limit of the Z range cannot be the same for each altitude has meeting ice hydrometeors linked to 15 dBZ or linked to -20dBZ at 200K is quiet impossible. The second fact holds on result on a former study (Cetrone and Houze 2009) which shows that distributions of Z as function of altitude are not the same in convective and stratiform part of MCS. This former study was performed with the 13GHz radar profiler on board TRMM satellite (Tropical Rainfall Measuring Mission), which is more sensitive to the precipitating particles (large drops and large ice crystals). The radar used in our study is more sensitive to smaller size of hydrometeors, then it is more adapted to the properties of ice crystals presented in our study.

We do not think that only MCS reflectivity zones can give information about the stage of the MCS in its life cycle (i.e. Formation, maturation, decaying), analyse of geostationary satellites would be more helpful for this topic (Folleau and Roca 2013). But, studying the distribution of MCS reflectivity zones as function of life cycle of MCS and brightness temperature and/or visible reflectance would be interesting for a future study.

MCS reflectivity zone has to be seen as a recalling of Z, but it add the information of the place of the Z among the distribution of Z in MCS (not for all of clouds).

Yes, it seems that the dynamic in lower MCS reflectivity zones is similar (i.e. 2, 3, 4 and 5), that could be put in a same class. But these class do not have the same range of IWC, visible extinction etc...

So put all the lower class of MCS zones together would bring less accurate profiles of the microphysic parameters.

We propose to re-write a part of the section 3.1 (from line 3 page 4 to the end of the section; R2#2):

“Figure 1 shows that distributions of Z are not totally similar for all 4 airborne campaigns. MCS can extend over hundreds or thousands square kilometres, where size and repartition of their convective and stratiform areas can vary from one MCS to another. So the same sampling strategy in two different MCS would provide two different mean or median profiles of ice microphysics properties as function of T. But two different sampling strategy in the same MCS would have the same results. The idea of this study is to compare the properties of ice hydrometeors

for different tropical MCS locations, thereby rendering comparable different MCS systems (as a function of temperature), through the analysis of the frequency distribution of profiles of Z dividing all MCS into eight zones. This strategy aims to reduce the impact of the different flight patterns and objectives for sampling MCS during each airborne campaigns used in this study.

Note that Z at 94 GHz is linked to the ice water content (Fontaine et al., 2014; Protat et al., 2016), but also to the size distribution of ice hydrometeors, respective crystal sizes, and mean diameter (Delanoë et al., 2014).

Our motivation to choose the limits of Z ranges on what the statistic of ice hydrometeors properties holds in two facts. First, Figure 1 shows that the variability of Z at a given T is large and this variability of Z vary along the altitude. We can observe in Figure 1 that Z extend from about -20dBZ to 18 dBZ at 260K while it spread out from -10dBZ to 10 dBZ at 200K. So, this has to be considered if we want to sort our dataset as function of T and Z. So the limit of the Z range cannot be the same for each altitude has meeting ice hydrometeors linked to 15 dBZ or linked to -20dBZ at 200K is quiet impossible. The second fact holds on result on a former study. Indeed, Cetrone and Houze, (2009) used the profiling radar of TRMM satellite ((Tropical Rainfall Measuring Mission; Huffman et al., 2007) to demonstrate with frequency distributions of radar reflectivity Z as a function of height that higher Z occur more often in convective echoes of MCS (in West African Monsoon, Maritime Continent and Bay of Bengal) than in their stratiform echoes. This former study was performed with the 13GHz radar profiler on board TRMM satellite, which is more sensitive to the precipitating particles (large drops and large ice crystals). The radar used in our study is more sensitive to smaller size of hydrometeors, then it is more adapted to sort the properties of ice crystals presented in our study. Hence, this study presents ice microphysical properties in MCS as a function of temperature layers and also as a function of zones of reflectivity Z. In order to fix the limits of a limited number of Z levels, this study takes the percentiles of all merged campaigns datasets shown by the solid lines (all data) in Figure 1. This defines Z ranges as a function of height. Hereafter, these ranges will be called MCS reflectivity zones and numbered 1 to 8:

- MCS reflectivity zone 1: $Z < Z^{1th}$
- MCS reflectivity zone 2 : $Z \in [Z(T)^{1th} ; Z(T)^{10th}[$
- MCS reflectivity zone 3 : $Z \in [Z(T)^{10th} ; Z(T)^{30th}[$
- MCS reflectivity zone 4 : $Z \in [Z(T)^{30th} ; Z(T)^{50th}[$
- MCS reflectivity zone 5 : $Z \in [Z(T)^{50th} ; Z(T)^{70th}[$
- MCS reflectivity zone 6 : $Z \in [Z(T)^{70th} ; Z(T)^{90th}[$
- MCS reflectivity zone 7 : $Z \in [Z(T)^{90th} ; Z(T)^{99th}[$
- MCS reflectivity zone 8 : $Z \geq Z(T)^{99th}$

”

And add these comments in the conclusion line 35 page 25 (R2#3):

“We do not think that alone, MCS reflectivity zones can give information about the stage of a MCS in its life cycle (i.e. Formation, maturation, decaying). The analysis of geostationary satellites data would be more suited for this topic (Fiolleau and Roca 2013). But, studying the distribution of MCS reflectivity zones as function of life cycle of MCS and brightness temperature and/or visible reflectance could be a future investigation. However, this study demonstrates...”

Paper length:

At the beginning of section 5 you introduce the general outline of Figures 5, 6, and 8 - 16, which I found a very good idea to keep the description of each figure short.

However, Section 5 still is too long! I would suggest to closely check from which figures/subsections you draw major conclusions and move those that only bear minor conclusions into a supplement and mention the investigation of the respective parameter in 1-2 sentences in the main manuscript. This will keep the manuscript more focused and the reader's attention. I will give some suggestions below, but you might want to identify other sections that could be moved yourself.

We propose to rewrite the section 5. First we take into account the comment about total concentrations, and remove the part talking about NT to put it in an appendices. But we keep the part concerning the mass-size coefficient. Secondly, we removed the part of the section 5 dedicated to the two parameterization, to do a section only dedicated to this topic. Note that figures have been remade due to reviewer 1 comments.

(R2#4)

5 In-situ Observations in tropical MCS: HAIC-HIWC and Megha-Tropiques projects

5.1 Ice water content

This section discuss about IWC measured during HAIC-HIWC project and the IWC retrieved for the Megha-Tropiques project. IWC from the four dataset were merged to calculate the main statistic (merged dataset). Figure 5 shows median IWC for the merged dataset as a function of T and as function of MCS reflectivity zones (colored lines). Solely, the graphical representation is limited to medians of IWC for MCS reflectivity zones 4 to 8. Indeed, IWC in MCS reflectivity zones 2 and 3 are linked to IWC smaller than 0.1 g m^{-3} , where IWC data are subject to less confidence. Globally, 30% of the data observed in 4 tropical MCS have an IWC lower than 0.1 g m^{-3} , and the lower limit of MCS reflectivity zone 4 is defined with the 30th percentiles of Z . The figure reveals an IWC increases with increasing MCS reflectivity zone for a given range of temperature. IWC median values differ clearly as a function of the MCS reflectivity zone, and this for the entire range of temperatures, with only a few exceptions above the freezing level ($T \in [265 \text{ K}; 273 \text{ K}]$), between MCS reflectivity zones 4 and 5, and MCS reflectivity zones 7 and 8, respectively, with small overlap in IWC ranges. In MCS reflectivity zones 4 to 7, median IWC increase with increasing T between 215 K and 260 K (where IWC has its maximum) and then slightly decrease as T further increases towards 273K. In MCS reflectivity zone 8 IWC behaves rather similar with a maximum IWC already reached at 250 K.

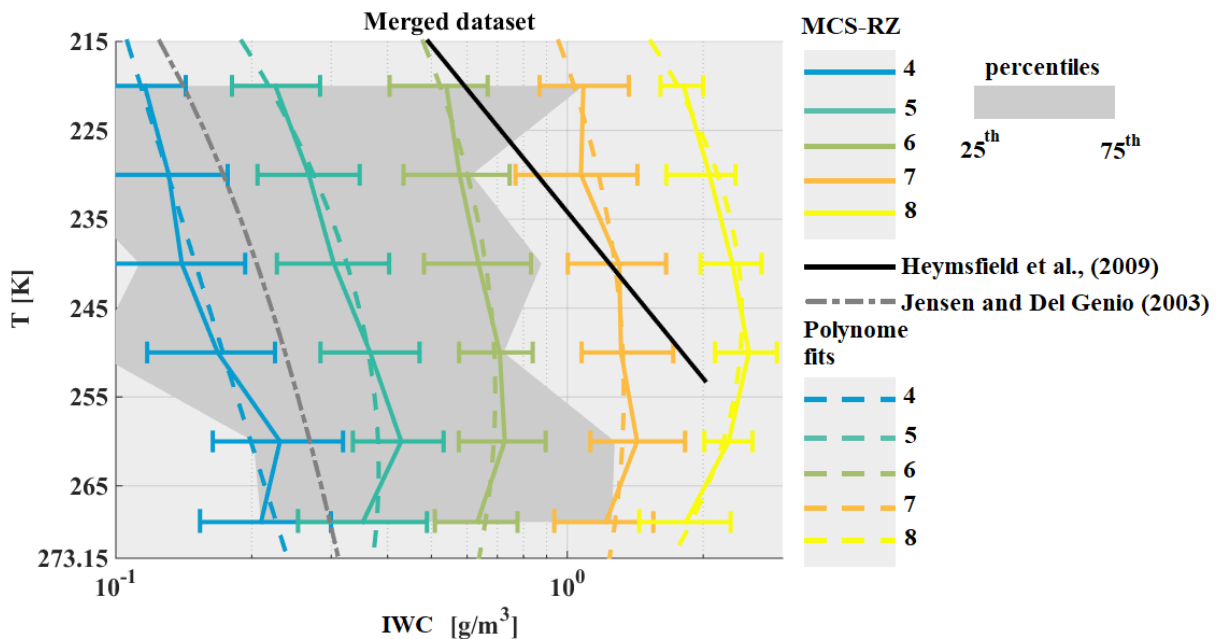


Figure 5: Median of IWC in $[\text{g/m}^3]$ on x-axis, as a function of temperature in $[\text{K}]$ on y-axis for different MCS reflectivity zones. Results for the merged dataset including both MT and both HAIC-HIWC datasets. The grey band represents 25th and 75th percentiles of merged dataset. Extremity of error bar show 25th and 75th percentiles of IWC in each MCS-RZ.

Figure 6 shows MRD-IWC for the four different campaigns. It is necessary that we recall that median IWC as function of T and MCS reflectivity zones are calculated using a merged dataset where there are IWC from direct measurement and retrieved IWC (Fontaine et al., 2017). Then, there is two different uncertainties (grey bands) to consider to evaluate the MRD-IWC in each campaigns. Firstly, for Darwin and Cayenne campaigns the IWC were measured with IKP-2 probe (direct measurement) with an uncertainty on measured IWC increasing with temperature ($\sim 5\%$ at 220K and $\sim 20\%$ at 273.15 K; Strapp et al., 2016). Secondly, for Niamey and Maldives IWC were retrieved using the method described by Fontaine et al., (2017) (indirect measurement) with an uncertainty with regards to the IKP estimated by about $\pm 32\%$. Hence, in Figure 6-a) and Figure 6-b) the grey band area show the uncertainty of the IKP-2 probe that was used for Cayenne and Darwin campaigns. While in Figure 6-c) and Figure 6-d) the grey band area describe the uncertainty on the retrieval method for IWC that was used for Niamey and Maldives.

Note that confidence in direct bulk IWC measurements from the IKP-2 is significantly higher than in indirect IWC calculations from the retrieval method (Fontaine et al., 2017).

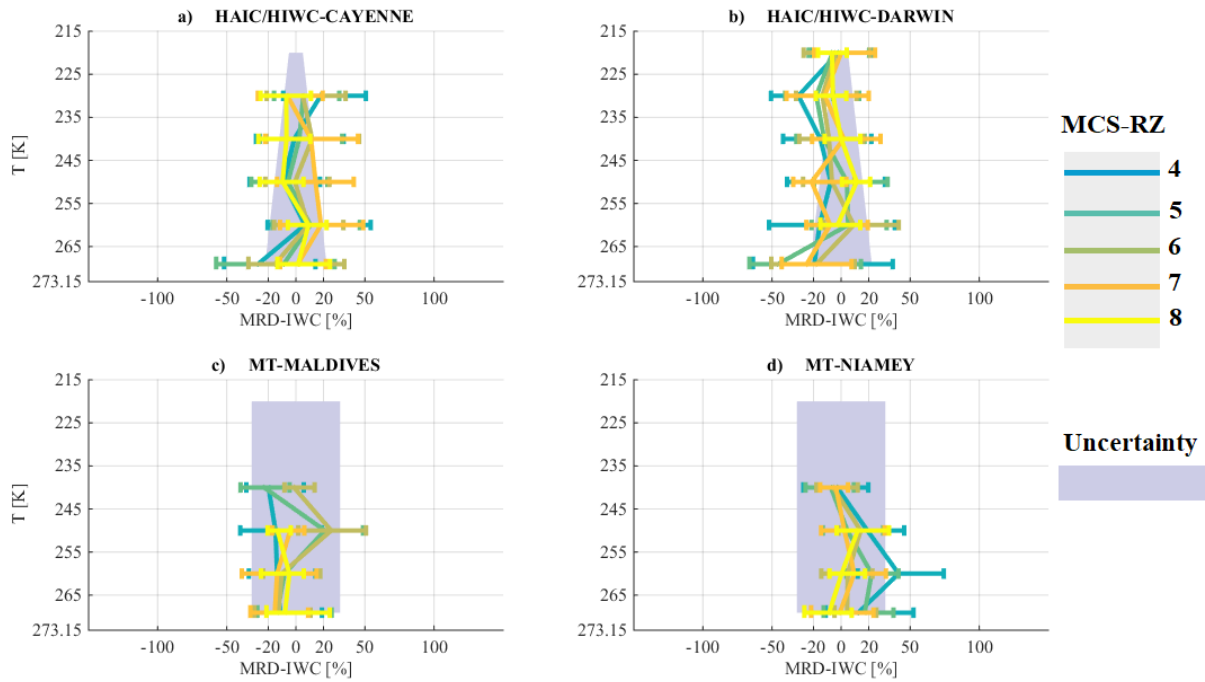


Figure 6: Median relative difference (MRD) of IWC during a) HAIC-HIWC in Cayenne, b) HAIC-HIWC in Darwin, c) Megha-Tropiques Maldives Islands and d) Megha-Tropiques in Niamey, with respect to median of IWC for the Tropical dataset on x-axis as a function of temperature in [K] on y-axis. The grey bands represent the uncertainties of the IWC measurement in b) and c), and the median deviation between measurement and the IWC retrieval method (Fontaine et al. 2016) in d) and e). Lines are colored as a function of the MCS reflectivity zones where in-situ measurement were performed, dashed colored lines are corresponding to the polynomial fit. Extremity of error bar show 25th and 75th percentiles of IWC relative error in each MCS reflectivity zone.

In addition, Figure 6(a), (b), (c), and (d) show MRD-IWC for all MCS reflectivity zones as a function of T . For all 4 tropical MCS, MRD-IWC in MCS reflectivity zones 4 to 8 are distributed around 0 and are in general less than 30-40% (25th to 75th percentiles). Measured IWC in MCS reflectivity zone 8 are in particular good agreement with the median IWC for all 4 tropical datasets, except maybe for high altitude MT-Niamey data. Uncertainty $U(IWC)/IWC$ for IKP-2 measurements (Darwin and Cayenne) especially at high altitude (about 5%) is smaller than the expected deviation MRD-IWC. For mid and lower altitudes, MRD-IWC for Darwin and Cayenne particularly for zones 5 and 8 are of the order of corresponding $U(IWC)/IWC$. Concerning, MCS over Niamey and the Maldives Island, MRD-IWC (25th to 75th percentiles) in general do not exceed corresponding $U(IWC)/IWC$.

For comparison purposes with former studies, two IWC- T relationships from literature are added in Figure 5(a). Jensen and Del Genio (2003) suggested an IWC- T relationship in order to account for the limited sensitivity of the precipitation radar aboard the TRMM satellite, not allowing for small ice crystals at the top of convective clouds' anvils to be observed. They used radar reflectivity factors of a 35GHz radar based on Manus Island (North-East of Australia; 2.058°S, 147.425°E), thereby calculating IWC from an IWC- Z relationship ($IWC=0.5*(0.5*Z^{0.36})$; Jensen et al., 2002). The resulting IWC- T relationship given by Jensen and Del Genio (2003) is reported by a dashed-dotted grey line, which fits between 75th percentiles of merged median IWC of MCS reflectivity zone 4 and 25th percentile of MCS reflectivity zones 5. We recall that IWC, as a function of T , in MCS reflectivity zones 4 and 5 are related to Z between 30th-50th and 50th-70th percentiles, respectively. We may notice that the IWC- T relationship from Jensen and Del Genio (2003) is different and smaller than the median IWC (4 tropical campaigns). Hence, IWC- T relationship from Jensen and Del Genio (2003) is more adapted to stratiform part of MCS where convective movement occurs less often.

Moreover, Heymsfield et al., (2009) established an IWC- T relationship based on 7 fields campaigns (black line in Figure 5). They focused their study on maritime updrafts in tropical atmosphere for a temperature range $T \in [213.15K; 253.15K]$. Their suggested IWC tend to be in the range of IWC of MCS reflectivity zones 6- 8 with IWC

increasing with T . We already showed in section 3.2 that MCS reflectivity zones 7 and 8 have higher probabilities to be convective (updraft regions with higher magnitudes of vertical velocity), as compared to other MCS reflectivity zones. Therefore, Heymsfield et al., (2009) IWC parametrizations for maritime updrafts are not inconsistent with data from this study.

Overall, this section demonstrates that variation of IWC with the temperature is similar in all type of MCSs for corresponding ranges of radar reflectivity factors. Hence, we assume that IWC-Z-T relationships developed in Protat et al., (2016) is usable for all types of MCS in the Tropics, at least for IWC larger than 0.1 g m^{-3} .

5.2 Visible extinction

Figure 7 shows visible extinction coefficients (σ) calculated from OAP 2D images (approximation of large particles; Van de Hulst, 1981):

$$\sigma = 2 \cdot \sum_{15\mu\text{m}}^{12845\mu\text{m}} N(D_{max}) \cdot S(D_{max}) \cdot \Delta D_{max} \quad [\text{m}^{-1}] \quad (1)$$

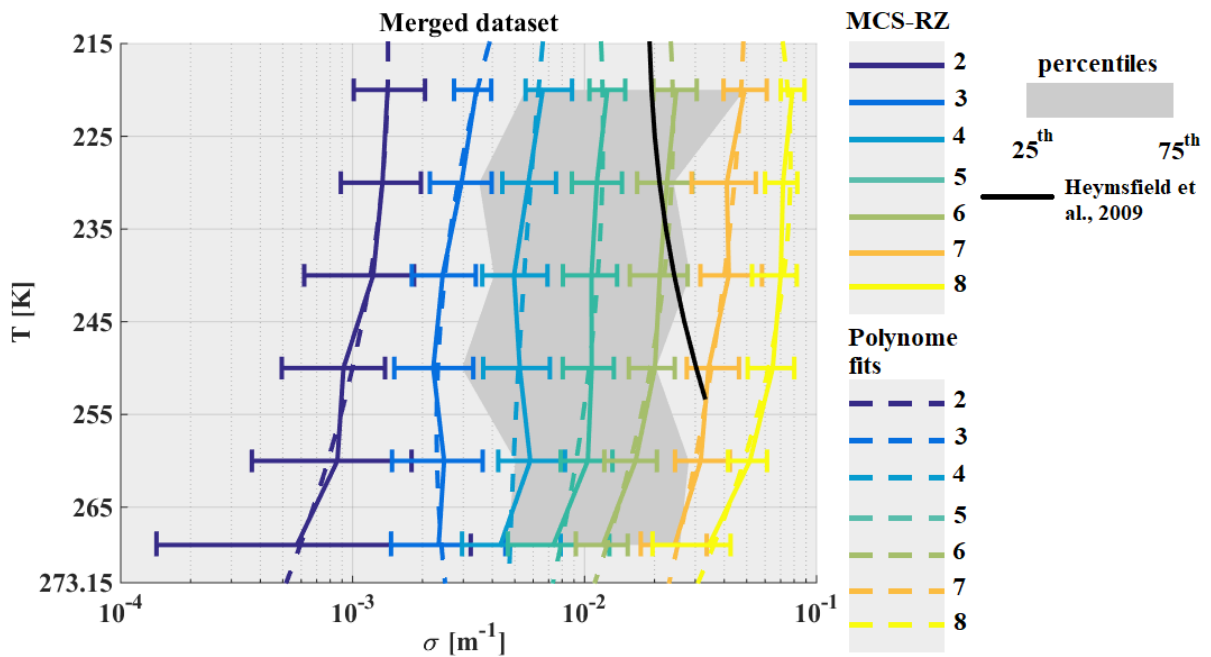


Figure 7: Same as Figure 5 but for visible extinction σ given on x-axis in m^{-1} .

In Figure 7, median σ (4 tropical campaigns) increase with MCS reflectivity zone as expected, and also increase with altitude (decrease with T), with larger gradients for $T \in [245; 273.15]$ than for $T \in [215\text{K}; 245\text{K}]$.

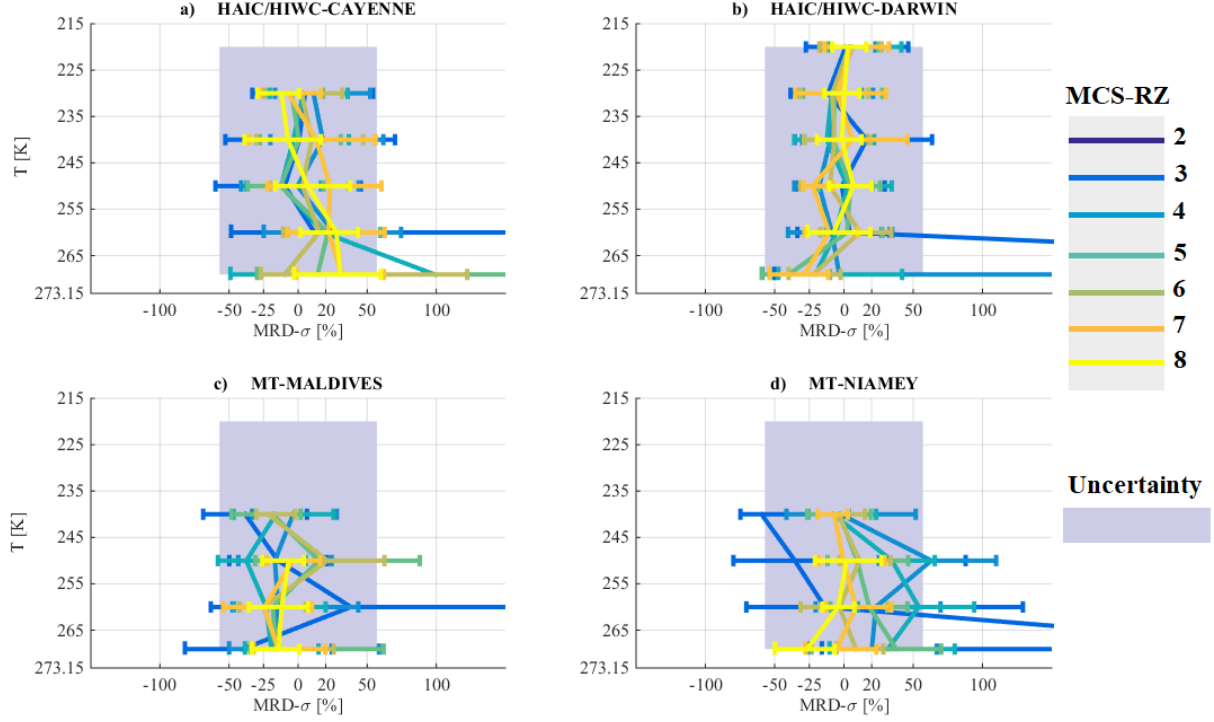


Figure 8: Same as Figure 6 but for visible extinction $MRD-\sigma$.

The uncertainty ($U(\sigma)/\sigma$) (grey band in Figure 8(a) to Figure 8(d)) is calculated as follows:

$$\frac{U(\sigma)}{\sigma} = \sqrt{2 \cdot \frac{U(D)^2}{D} + \frac{U(N)^2}{N}} = \pm 57\% \quad (2)$$

With $\frac{U(D)}{D} = \pm 20\%$, taking into account the uncertainty in the calculation of the size of hydrometeors and $\frac{U(N)}{N} = \pm 50\%$ for the uncertainty on the calculation of the concentration of hydrometeors from optical array probes (Baumgardner et al., 2017). Above uncertainties are those for particles larger than $100 \mu\text{m}$. Note, that if we took uncertainties for particles smaller than $100 \mu\text{m}$ (with $\frac{U(D)}{D} = \pm 50\%$ and $\frac{U(N)}{N} = \pm 100\%$) the uncertainty on the calculation of σ would increase to $\pm 122\%$. The reason why we do not take into account uncertainty of smaller particle it is because these particles contribute little to the visible extinction (2% in the range [235K; 273.15] and 10% in the range [215K; 225K].”

For all 4 types of tropical MCS, $MRD-\sigma$ shown in Figure 8(a), 8(b), 8(c), and Figure 8(d) are in general smaller or equal to $\pm \frac{U(\sigma)}{\sigma}$. Hence, visible extinction in tropical MCS tend to be similar for all types of MCS observed in the same range of T and MCS reflectivity zone. Also $MRD-\sigma$ trends are very comparable to above discussed $MRD-IWC$ trends.

Furthermore, a $\sigma-T$ relationship from Heymsfield et al. (2009) (black line) is added in Figure 7, which is calculated, as a function of T, as the sum of the total area of particles larger than $50 \mu\text{m}$ plus the total area of particles smaller than $50 \mu\text{m}$ multiplied with a factor of 2 in order to satisfy Eq. (1) and to compare with results of this study. We conclude that $\sigma-T$ estimation presented in Heymsfield et al. (2009) for maritime convective clouds is rather comparable to median σ calculations (merged dataset) in MCS reflectivity zones 6 to 7 corresponding to higher reflectivity zones, and thus statistically to zones with some remaining convective strength.

5.3 Concentration of ice hydrometeors

Subsequently are presented observed total concentrations for the merged datasets integrating particle sizes beyond $55 \mu\text{m}$ ($N_T(D_{max} > 55 \mu\text{m})$); hereafter $N_{T,55}$:

$$N_T(D_{max} > 50\mu\text{m}) = \sum_{D_{max}=55}^{D_{max}=12845} N(D_{max}) \cdot \Delta D_{max} \quad [L^{-1}] \quad (3)$$

Median of $N_{T,55}$ as a function of T and MCS reflectivity zones are shown in Figure 9 as well as MRD- $N_{T,55}$ for the 4 tropical MCS locations in Figure 10 (a), 10(b), 10(c), and 10(d). We observe an increase of median $N_{T,55}$ with altitude for all MCS reflectivity zones. Also $N_{T,55}$ increases with MCS reflectivity zones for a given T , with highest $N_{T,55}$ in MCS reflectivity zone 8. The range of variability for $N_{T,55}$ reveals significant overlap of 25th and 75th percentiles of neighboring MCS reflectivity zones.

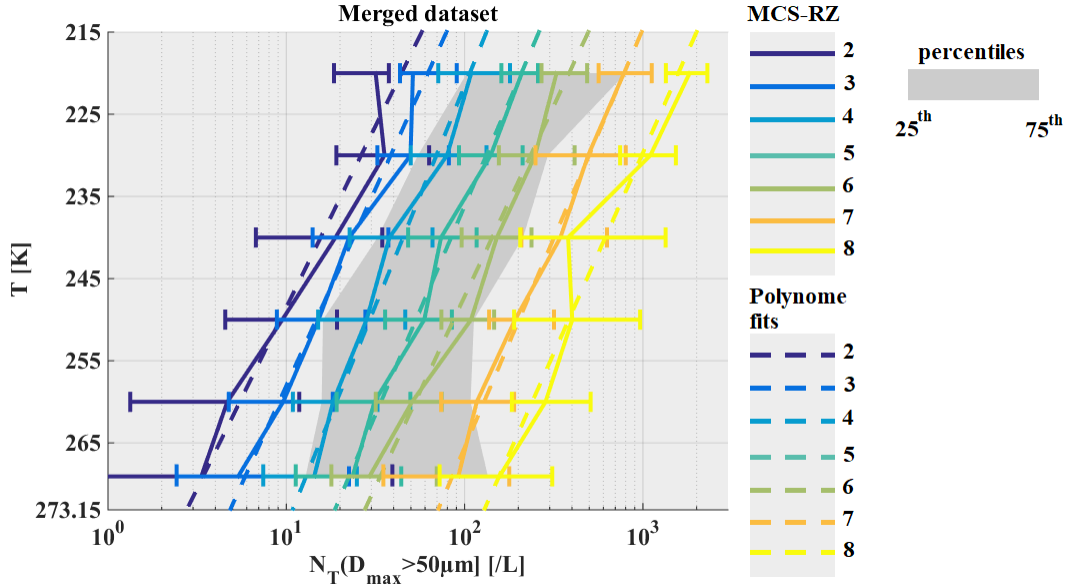


Figure 9: Same as Figure 5, but for total concentrations integrated beyond $D_{max}=55\mu\text{m}$ in $[L^{-1}]$.

Figure 10 show MRD- $N_{T,55}$ where measurement uncertainty on concentrations are assumed $\pm 100\%$ (Baumgardner et al., 2017). MRD- $N_{T,55}$ in 4 different tropical MCS locations, particularly for higher MCS reflectivity zones are of the order and even larger (75th percentile MRD- $N_{T,55}$) than the measurement uncertainty. Even if the limit of concentrations of ice hydrometeors are not well defined between neighboring MCS reflectivity zones (Figure 9). These concentrations tend to be similar for a given range of T and Z for the four different MCS locations.

A similar investigation is performed for total concentrations integrating beyond $15\mu\text{m}$ (N_T). Since major conclusion are similar to these given for $N_{T,55}$, figures for N_T are shown in Appendices A. Globally, median of $N_{T,55}$ for the tropical dataset are smaller by about one order of magnitude with respect to the median of N_T for the same MCS reflectivity zone. And N_T over Maldives tend to be larger than median N_T for the merged dataset.

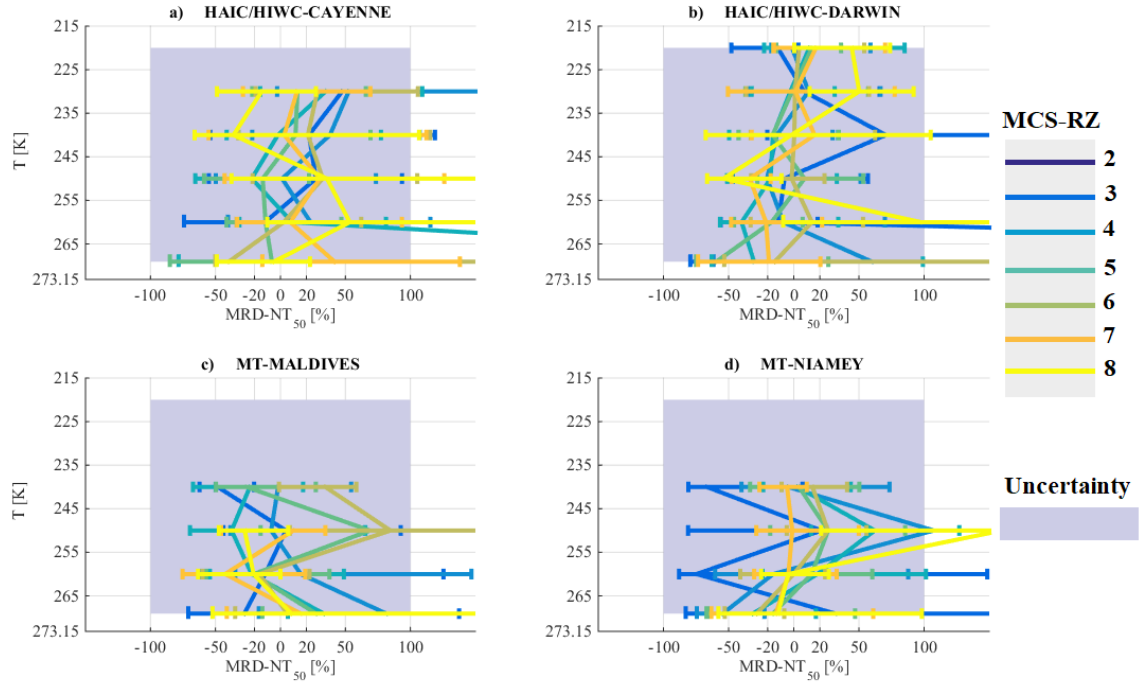


Figure 10: Same as Figure 6, but for MRD-NT₅₀.

Finally, Figure 11 shows concentrations of hydrometeors when number PSD are integrated only beyond 500 μm (hereafter $N_{T,500}$; eq. (4)), where the uncertainty on their measurement is estimated as about $\pm 50\%$ for hydrometeors larger than 100 μm (Baumgardner et al., 2017).

$$N_T(D_{max} > 500\mu\text{m}) = \sum_{D_{max}=505}^{D_{max}=12845} N(D_{max}) \cdot \Delta D_{max} \quad [L^{-1}] \quad (4)$$

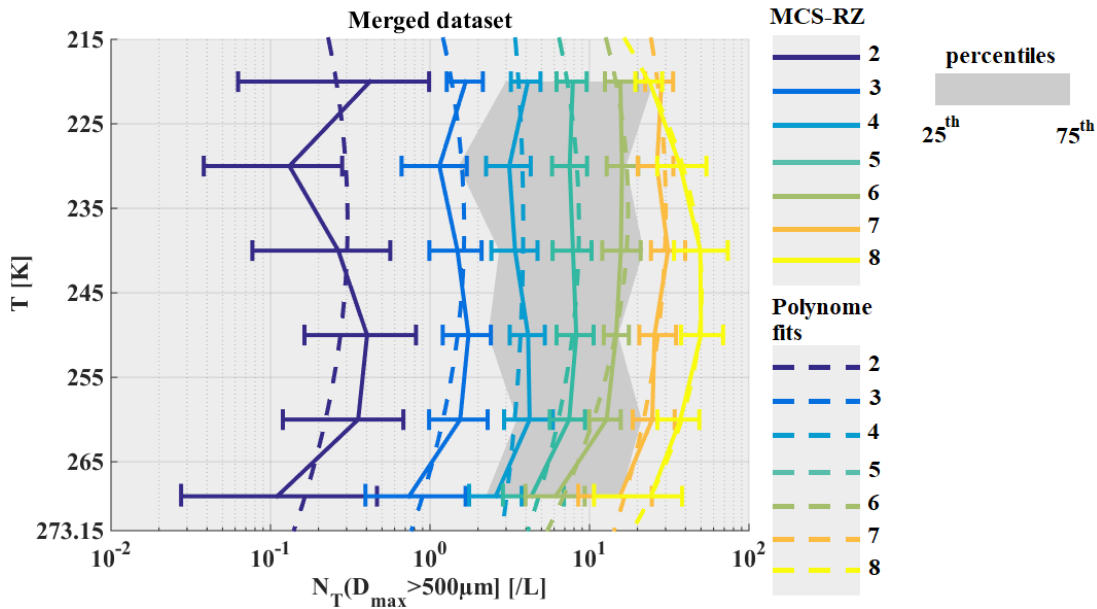


Figure 11: Same as Figure 5, but for concentrations of hydrometeors integrated beyond $D_{max} = 500\mu\text{m}$ in $[L^{-1}]$.

In Figure 11 median $N_{T,500}$ are presented as a function of T and MCS reflectivity zone. The curves of median $N_{T,500}$ are different from curves of median N_T and $N_{T,55}$. Indeed, particularly for higher MCS reflectivity zones and in lower altitude levels ($T \in [250\text{K}; 273.15\text{K}]$), $N_{T,500}$ tends to increase with altitude, reaches a maximum value

around $T \in [235K; 250K]$, and then rather decreases for $T \in [215K; 235K]$. The range of variability for $N_{T,500}$ reveals a rather small overlap, if any, of 25th and 75th percentiles of neighboring MCS reflectivity zones 8, 7, and may be 6, mainly at coldest $T \in [215K; 225K]$. No overlap for MCS reflectivity zones 2-5 and concentration of ice hydrometeors beyond $500\mu\text{m}$ are rather constant from 215K to 265K for observations in MCS reflectivity zones 3 to 5. We can assume that sedimentation does not significantly impact hydrometeors of sizes below $500\mu\text{m}$, but should impact larger hydrometeors.

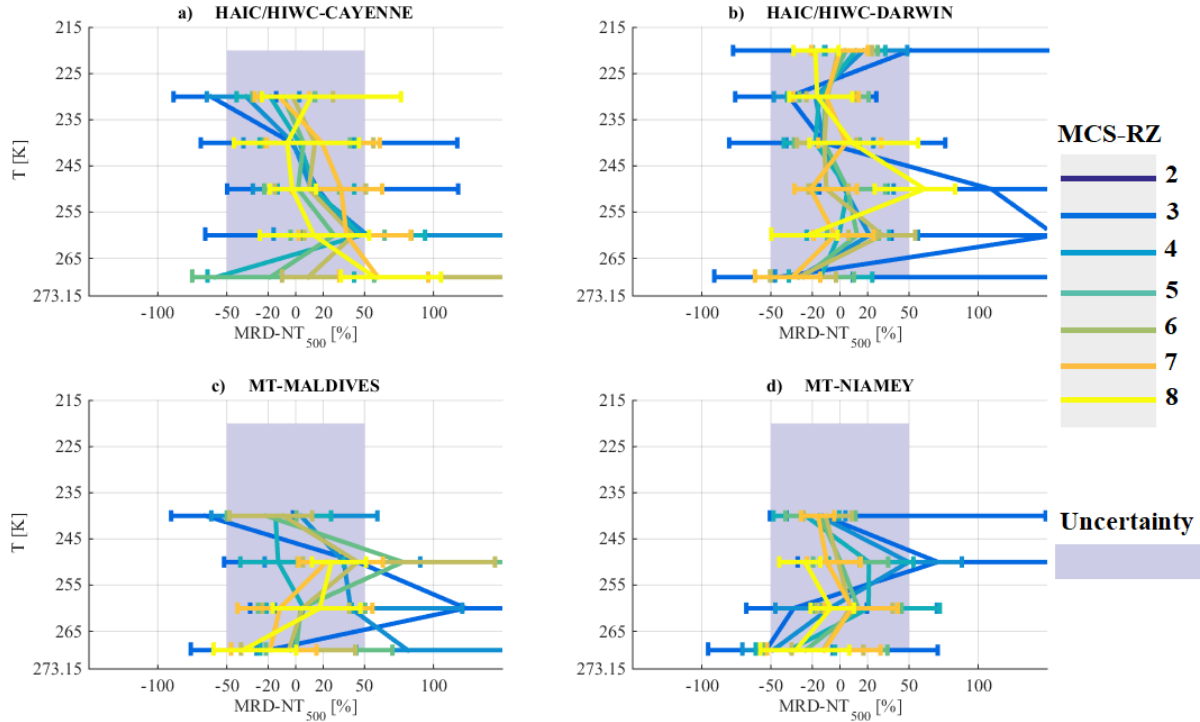


Figure 12: Same as Figure 6, but for $MRD-N_{T,500}$.

Figure 12 (a), 12(b), 12(c), and 12(d) reveal that $MRD-N_{T,500}$ in higher MCS reflectivity zones are considerably smaller or roughly equal to the measurement uncertainty for large hydrometeors. Some smaller exceptions are noticeable where $MRD-N_{T,500}$ are larger than the measurement uncertainty for very low altitudes at $T \in [265K; 273.15K]$, namely Cayenne in MCS reflectivity zones 7 and 8, and Darwin in MCS reflectivity zone 8. Note, that in general $MRD-N_{T,500}$ have smaller 75th percentiles (from Figure 10 (b), 10(c), 10(d), and 10(e)) compared to respective $MRD-N_{T,55}$ and $MRD-N_T$, showing that variability in each MCS reflectivity zone for hydrometeors larger than $500\mu\text{m}$ is smaller than the variability of concentrations which include smaller ($N_{T,55}$) and smallest (N_T) hydrometeors. This finding is clearly related to the uncertainty estimation given by (Baumgardner et al., 2017)) that small hydrometeors ($D_{max} < 100\mu\text{m}$) have a larger estimated uncertainty of 100% (due to shattering, very small sample volume), compared to the uncertainty of only 50% for larger hydrometeors ($D_{max} > 100\mu\text{m}$). Hence, it is not surprising that variability around a median value is larger for N_T and $N_{T,55}$ than for $N_{T,500}$. It is important to resume here that not just $MRD-N_{T,500}$ is smaller than the uncertainty of 50%, but also that $MRD-N_{T,500}$ is tremendously smaller than $MRD-N_{T,55}$ and $MRD-N_T$. Even though we have to keep in mind that we'll never have sufficient statistics in flight data, due to sampling bias of flight trajectories and variability of microphysics from one system to another. Indeed, Leroy et al., (2017) demonstrated that median mass diameter MMD_{eq} generally decrease with T and increasing IWC for the dataset of HAIC-HIWC over Darwin. However, for two flights performed in the same MCS, Leroy et al., (2017) showed that high IWC were linked to large MMD_{eq} , where MMD_{eq} tends to increase with IWC. This demonstrates that comparable high IWC can be observed for two different microphysical conditions (short-lived typical oceanic MCS versus long lasting tropical storm in one and the same dataset).

We show that total concentrations starting from $15\mu\text{m}$ can be different between MCS locations as a function of T and Z , especially in oceanic MCS over Maldives Islands in the decaying part of these MCSs where measured concentrations can reach 10 times the median concentrations observed globally for merged tropical dataset. Also MCS over Niamey show larger concentrations near the convective part of MCS. However, concentrations of ice

hydrometeors beyond 55 μm tend to be more similar as function of T and Z, even if the limits between each MCS reflectivity zones are not well defined.

Between 4 MCS locations, differences of aerosol loads and available ice nuclei might exist. Despite those possible differences, ice crystal formation mechanisms may be primarily controlled by dynamics, thermodynamics and particularly by secondary ice production rather than primary nucleation; (Field et al., 2016; Phillips et al., 2018; Yano and Phillips, 2011) that regulate the concentrations of hydrometeors beyond ~55 μm making these concentrations quiet rather similar for different MCS locations.

5.4 Coefficients of mass-size relationship

The relationship between mass and size of ice crystals is complex. Usually in field experiments the mass of individual crystals is not measured, instead bulk IWC is measured which is the integrated mass of an ice crystal population per sample volume to be linked to PSDs of ice hydrometeors. Yet IWC is not always measured or with low accuracy. Due to the complex shape of ice hydrometeors, various assumptions allow to estimate the mass of ice crystals for a given size. Indeed, many habits of ice crystals can be observed in clouds, primarily as a function of temperature and ice saturation (Magono and Lee, 1966; Pruppacher et al., 1998). Also hydrometeors of different habits can be observed at the same time (Bailey and Hallett, 2009). Locatelli and Hobbs (1974) and Mitchell (1996) suggested mass-size relationships represented as power laws with $m = \alpha \cdot D^\beta$ for different precipitating crystal habits. Coefficients α and β vary as a function of the ice crystals habit. Further studies performed calculations of mean mass-size relationships (also using power law approximations) retrieved from simultaneous measurements of particle images combined with bulk ice water content measurements (Brown and Francis, 1995; Cotton et al., 2013; Heymsfield et al., 2010). Schmitt and Heymsfield (2010), Fontaine et al (2014), Leroy et al. (2016) showed that mass-size relationship coefficients α and β vary as a function of temperature. In the latter studies, coefficient β is calculated from OAP images, and then α is retrieved either also from processed images or constrained with integral measured IWC or radar reflectivity factor Z. Recently, Coutris et al (2017) retrieved masses of hydrometeors by an inverse method using direct measurement of PSD and IWC. In this latter study, the mass of ice crystals is retrieved without any assumption on the type of function linking mass and size of ice hydrometeors.

This study uses the power law assumption to constrain the mass of ice hydrometeors. Thereby, the β exponent of the mass-size power law relationship is calculated (eq. 7) as presented in Leroy et al (2016) for hydrometeors defined by D_{max} dimension:

$$\beta = 1.71 \cdot f_s - 0.62 \cdot f_p \quad (5)$$

Here f_p is the exponent of the perimeter-size power law relationship (Duroure et al. 1994) with $P(D_{\text{max}}) = e_p \cdot D_{\text{max}}^{f_p}$ [cm] and f_s is the exponent of the 2D image area-size relationship (Mitchell, 1996) with $S(D_{\text{max}}) = e_s \cdot D_{\text{max}}^{f_s}$ [cm²]. These two relationships are calculated using Images from 2D-S and PIP. Hence, β is a proxy parameter that describe the global (all over the size range of hydrometeors from 50 μm to 1.2cm) variability of the shape of the recorded hydrometeors during the sampling process. Figure 13 shows the variability of β as a function of temperature and MCS reflectivity zones for the merged dataset. For a given MCS reflectivity zone, β increases with increasing temperature. Also for a given temperature, β increases with MCS reflectivity zone, although MCS reflectivity zones 4, 5, 6, 7, and 8 share a range of common values for β , making it more uncertain to predict with a good accuracy using a parametrization as function of IWC and T.

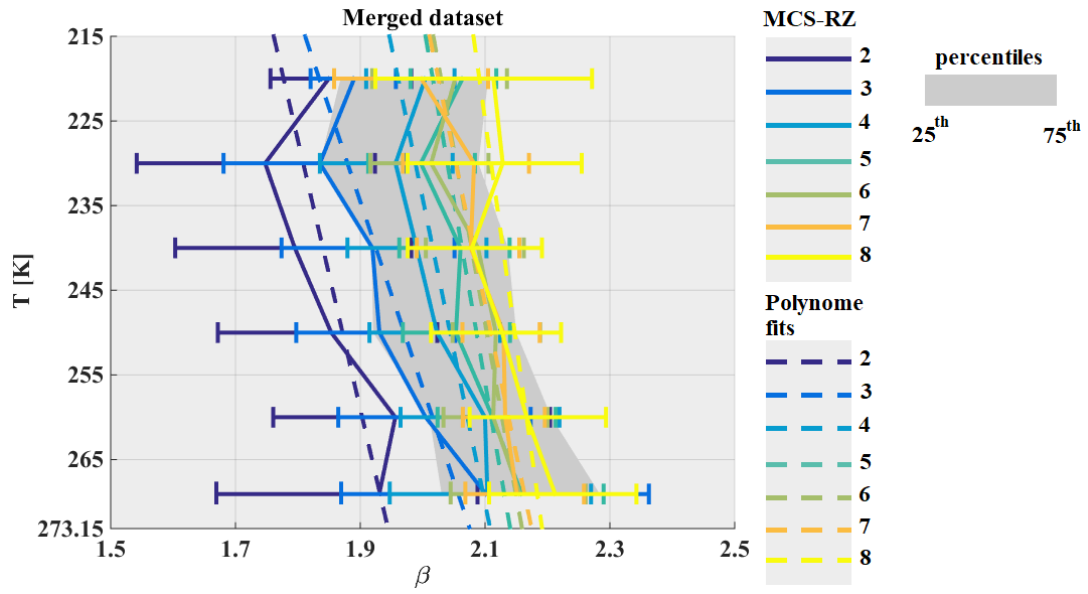


Figure 13: As Figure 5, but for exponent β of mass-size relationships for used ice hydrometeor size definition D_{max} .

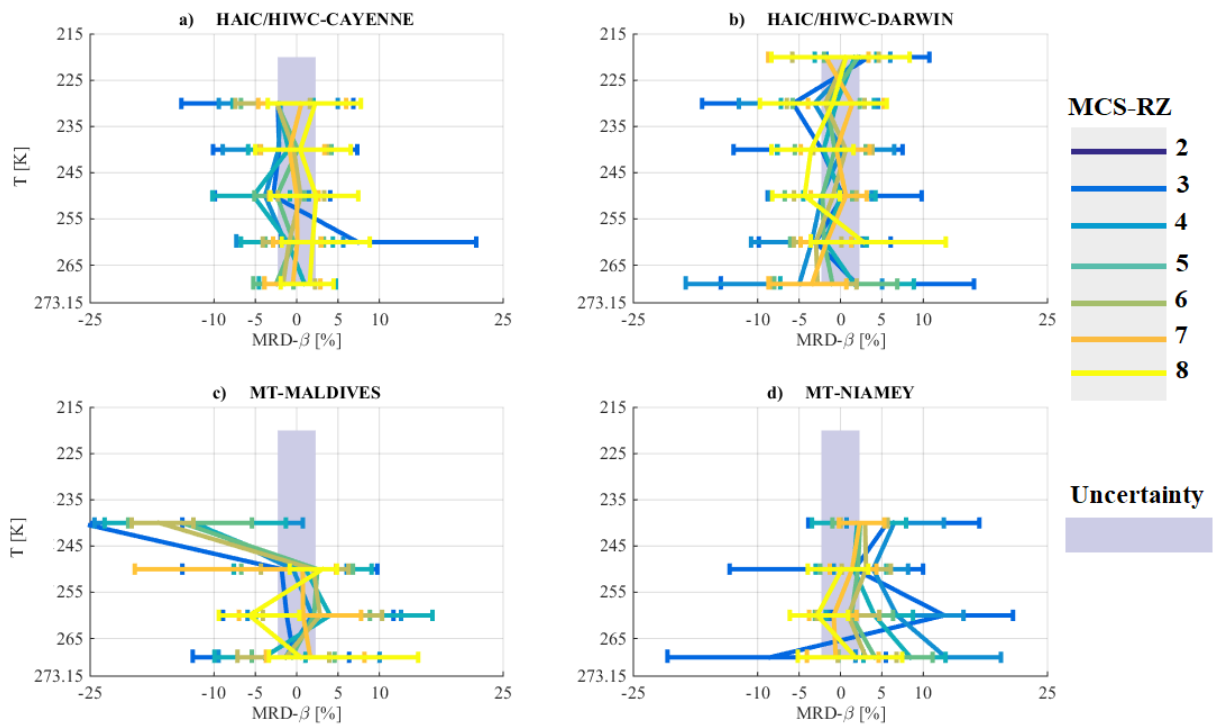


Figure 14: As Figure 6, but for exponent $MRD-\beta$.

In order to estimate the uncertainty on the calculation of β (grey band in Figure 14 (a), (b), (c), and (d), results from (Leroy et al., 2016) have been utilized, with $U(\beta)/\beta = \pm 2.3\%$. However, if we have calculated the uncertainty on retrieved β from the uncertainty on the measurement of the size and concentration of hydrometeors from OAP images, the uncertainty would have been by about 44%. In general, $MRD-\beta$ in MCS reflectivity zones 8 and 7 tend to be in the range of $U(\beta)/\beta$ assuming that β are similar for all observed MCS in the four campaigns for the conditions described by MCS reflectivity zones 7 and 8.

However, in MCS reflectivity zones 2 to 6 $MRD-\beta$ are more scattered around $U(\beta)/\beta$ with sometimes larger MRD than uncertainty of β . Especially for MCS over Maldives and Niamey. Over Maldives at higher altitudes β tend to

be smaller compared to the median β calculated for the merged dataset. While, MCS over Niamey tend to have β larger than median β calculated for the merged dataset.

Overall, the predictability of β coefficients as a function of T and MCS reflectivity zone remains challenging. We are aware of the fact that the power-law approximation has certain limits, trying to impose one single β to an entire crystal population composed of smaller (dominated by pristine ice) and larger crystals (more aggregation, also riming).

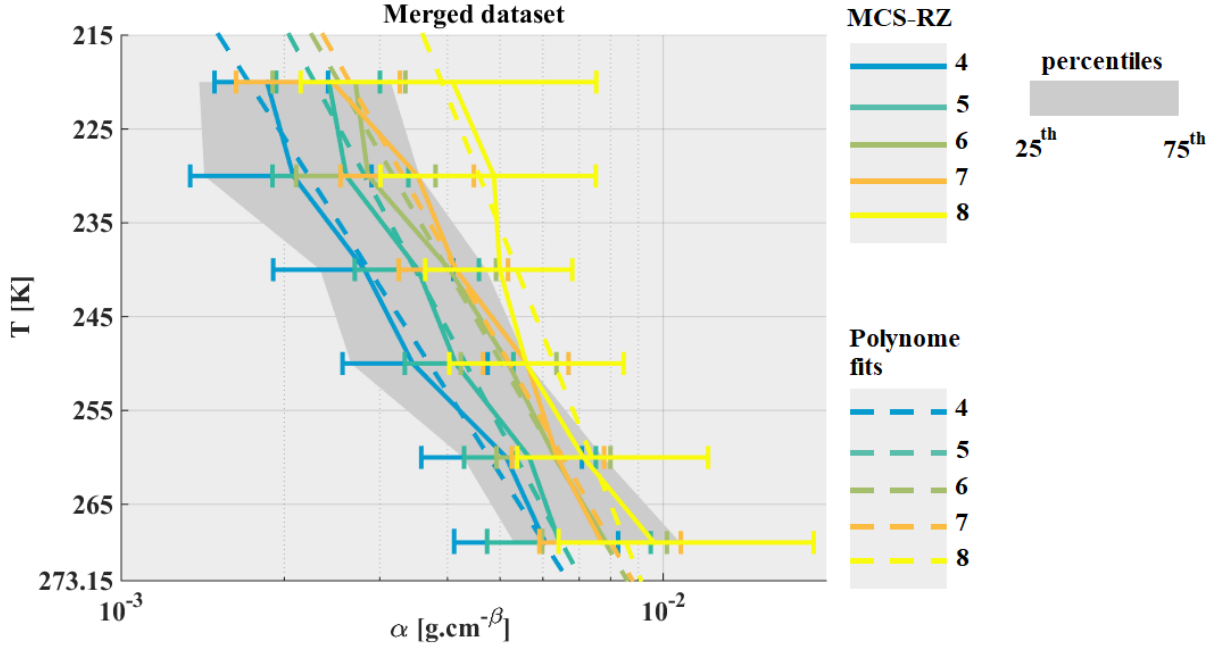


Figure 15: Same as Figure 5, but for α of mass-size relationships for used ice hydrometeor size definition D_{max} .

For HAIC-HIWC data, coefficients α are retrieved, while matching measured IWC from IKP-2 with calculated IWC thereby integrating PSD times $m(D)$ power law relationship. For MT data, coefficients α are retrieved from T -matrix simulations of the reflectivity factor (Fontaine et al., 2017). α calculation is solely constrained by the fact that the mass of ice crystals remains smaller or equal than the mass of an ice sphere with the same diameter D_{max} :

$$\alpha = \frac{IWC}{\sum_{15}^{12845} N(D_{max}) \cdot D_{max}^{\beta} \cdot \Delta D_{max}} \quad | \quad \alpha \cdot D_{max}^{\beta} \leq 0.917 \cdot \frac{\pi}{6} \cdot D_{max}^3 \quad [g \text{ cm}^{-\beta}]. \quad (6)$$

For the uncertainty calculation of α we take the maximum value of β which is 3:

$$\frac{U(\alpha)}{\alpha} = \sqrt{\left(\frac{U(IWC)}{IWC}\right)^2 + 3 \cdot \left(\frac{U(D)}{D}\right)^2 + \left(\frac{U(N)}{N}\right)^2} \quad (7)$$

Figure 15 shows median α coefficients as a function of T and MCS reflectivity zone. As has been already stated in previous studies, α is strongly linked to the variability of β (Fontaine et al., 2014; Heymsfield et al., 2010). Figure 15 compared to Figure 13 confirms that results for α have similar trends as those discussed for β . α vary from $5 \cdot 10^{-4}$ (in MCS reflectivity zone 2) to $\approx 2 \cdot 10^{-2}$ (in MCS reflectivity zone 8). In general, α increases as a function of T for a given MCS reflectivity zone and also increases as a function of MCS reflectivity zone (and associated IWC) for a given T level. As already stated for the median exponent β in Figure 13, median α in MCS reflectivity zones 4, 5, 6, 7 and 8 are more or less overlapping. Median α in MCS reflectivity zones 2 and 3 are shown for completeness reasons, however with less confidence as they are related to IWC generally smaller than $0.1 g m^{-3}$.

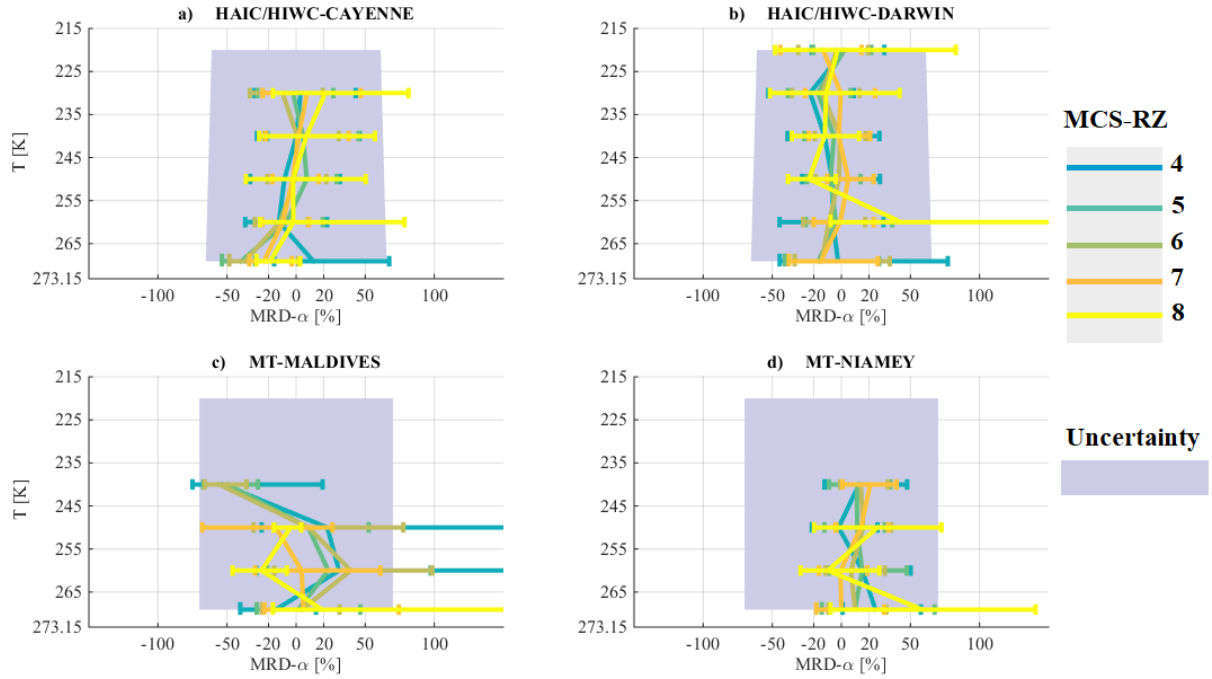


Figure 16: As Figure 6, but for exponent $MRD-\alpha$

From Figure 16(a) and Figure 16(b) we can note that even with a good accuracy of the measured IWC (from IKP-2; $U(IWC)/IWC \approx \pm 5\%$ for the typical IWC values observed in HAIC-HIWC at 210K), the uncertainty of α , is rather large which is mainly due to uncertainties in OAP size and concentration measurements. Taking into account the large uncertainty on the retrieved α , we find that $MRD-\alpha$ for all 4 tropical datasets for MCS reflectivity zones 4, 5, 6, 7, and 8 are smaller than $U(\alpha)/\alpha$. For data from Niamey (Figure 16 (d)), α tend to be larger than median α for the tropical dataset ($MRD-\alpha$ not centered on 0, but shifted to positive values).

In previous sections, this study documented similar IWC values and visible extinction coefficients for a given range of Z and T and a clear increase of IWC and visible extinction coefficient from MCS reflectivity zones 4 to 8. The increase of α and β with MCS reflectivity zones is not as much clearly visible, whereas at least α seems to increase with temperature in different MCS reflectivity zones. And we cannot ignore that α and β tend to be larger in MCS reflectivity zone 8 than in MCS reflectivity zone 4, especially at higher altitude. But, the increase of IWC and visible extinction with MCS reflectivity zone Z is not linked to an increase of the mass-size coefficients. This conclusion takes into account the variability of the mass-size coefficients shown by 25 and 75 percentiles. Moreover, shapes of ice hydrometeors in MCS reflectivity zone 4, 5 and 6 are different in MCS over Maldives and MCS over Niamey compared to MCS over Darwin and Cayenne (smaller β over Maldives and larger β over Niamey).

As visible extinction (hence projected surface) and IWC are similar for the same range of T and Z in all types of MCS, but the shapes of crystals might be different from one to another MCS location. Our assumption is that the ratio of projected surface vs IWC is similar. In other words the density of ice per surface unity (or by pixels of projected surface) is similar as function of T and Z in all types of MCS even if there might be a possibility that the habit or the shape can be different (pure oceanic MCS vs pure continental MCS). Note that these assumptions establish for IWC larger than 0.1 g m^{-3}

5.5 Largest ice hydrometeors

Figure 17 investigates the variability of the size of the largest ice hydrometeors in the PSD (hereafter $\max(D_{\max})$ as defined in Fontaine et al (2017)). Figure 17 reveals globally for all MCS reflectivity zones that the median of $\max(D_{\max})$ increases with T, with larger hydrometeors at cloud base compared to cloud top, particularly in the stratiform cloud part, where PSD are mainly impacted by a combination of aggregation and sedimentation. At higher levels for $T \in [215\text{K}; 245\text{K}]$ largest median of $\max(D_{\max})$ are observed in the most convective MCS reflectivity zone 8, followed by zones 7, 6, and 5, where sedimentation becomes more and more active. Below the 250K level, largest $\max(D_{\max})$ can be observed in MCS reflectivity zones 6 and 7 (still significant sedimentation source from above), followed by 5 (increasing depletion of large crystals) and 8 (more convective or at least

transition zone from convective to stratiform cloud part). Smallest $\max(D_{\max})$ are observed in MCS reflectivity zones 2 and 3.

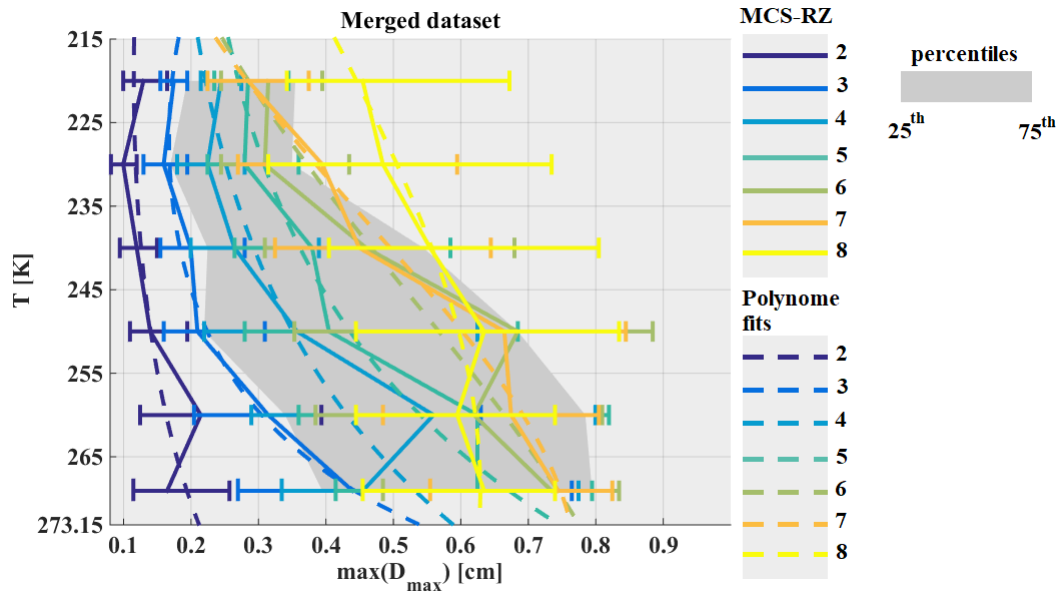


Figure 17: As Figure 5, but for maximum size of hydrometeors $\max(D_{\max})$ in PSD in [cm].

$MRD-\max(D_{\max})$ shown in Figure 18(a), 18(b), 18(c), and 18(d) are a bit larger than the measurement uncertainty estimated with $\pm 20\%$ (Baumgardner et al., 2017). Cayenne, Darwin, and Niamey data are centered around the median $\max(D_{\max})$ of the 4 tropical datasets in MCS reflectivity zone 8 for all type of MCSs, in MCSs reflectivity zone 7 in MCS over Darwin, Cayenne and Niamey. MCSs over Cayenne et Darwin tend to have similar $\max(D_{\max})$ in other MCS reflectivity zones. Maldives dataset shows mainly negative $MRD-\max(D_{\max})$ values, indicating that $\max(D_{\max})$ for the Maldives Island data are generally smaller than those of the other three tropical datasets. Also MCS over Niamey show larger $\max(D_{\max})$ in MCS reflectivity zones 2 to 4, illustrating that snow aggregates can reach larger sizes during the West African monsoon than in other MCS locations.

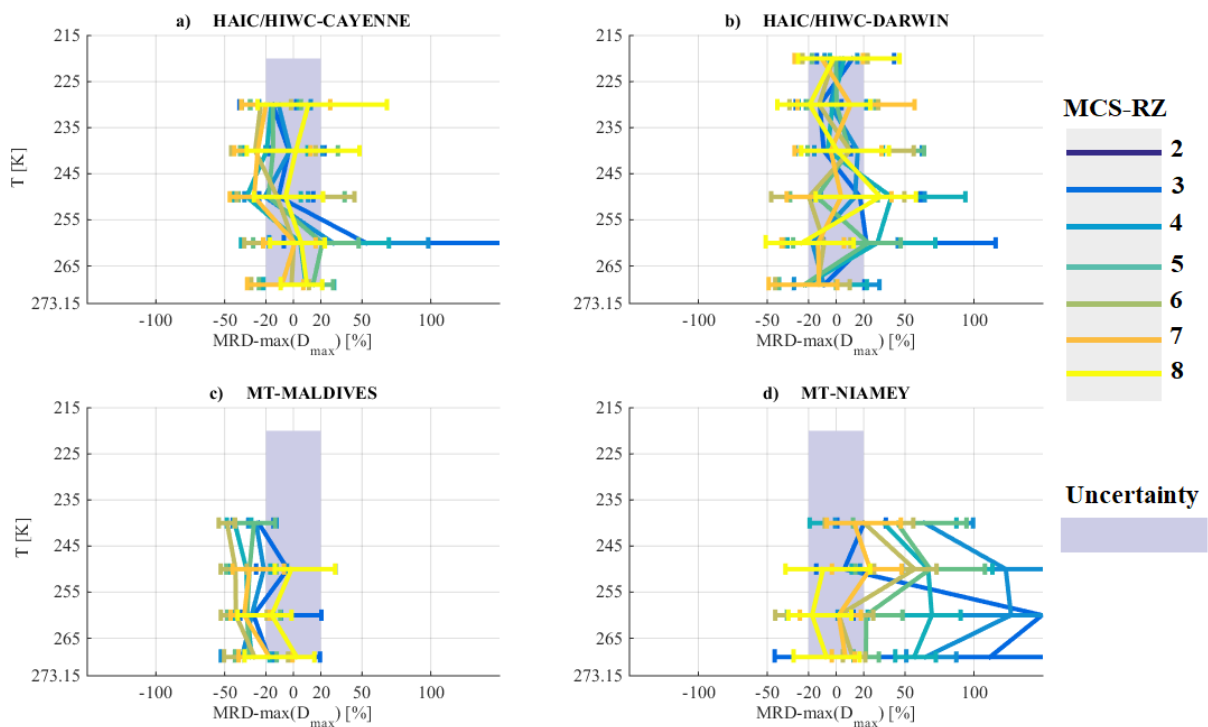


Figure 18: As Figure 6, but for maximum size of hydrometeors $\max(D_{\max})$

In this section, it is shown that in the stratiform part of MCS, largest hydrometeors are larger in MCSs over Niamey than in other types of MCS, and tend to be smaller in MCS over Maldives Islands. Mainly, large crystals ($D_{\max} > 1\text{mm}$) are agglomerates of pristine ice crystals, for which the growth process is leaded by aggregations (by sedimentation) instead of vapour diffusion. Some large pristine ice were found in the dataset (especially over Maldives see Figure 1 in Fontaine et al., 2014) but usually their size do not exceed 3 to 4 mm. Hence, aggregation efficiency is different from one MCS type of MCS to another, this could explain the differences of mass-size coefficient β , as it is calculated on the slope in a log-log scale of mean perimeter and mean surface as a function of median diameter in each size bin. Because, large hydrometeors have a non-negligible impact on the slope (i.e. f_p and f_s , see Eq. (5)).

5.6 note on the impact of vertical movement on ice microphysic

This section discussed about the investigation performed about the impact of vertical velocity on the ice microphysical parameters presented earlier in this section 5. We separated the merged dataset in three sub-datasets such: i) $w < -1\text{m/s}$, (ii) $-1\text{m/s} < w < 1\text{m/s}$ and (iii) $w > 1\text{m/s}$. Then, median relative difference for the three conditions and for each parameters presented in this section 5 were calculated and compared to the median relative difference when no distinction is performed as function of vertical velocity. Firstly, we noticed that MRD-X for the merged dataset and MRD-X for the second condition (i.e. $1\text{m/s} < w < 1\text{m/s}$) are similar (MRD-X: X being used to replace IWC, σ , NT, NT_{50} , NT_{500} , β , α , $\max(D_{\max})$). Secondly, differences of MRD-X in updraft and in downdraft with regards to MRD-X for merged dataset and no vertical movement are visible. But most of the times these differences are not enough pronounced compared to measurement uncertainties ($U(X)/X$).

Appendices B shows the Figures that shows when updraft have an impact on ice microphysic parameters for a given range of temperature and MCS reflectivity zones. So, Figure B1 shows MRD-IWC, Figure B2 shows MRD-NT and Figure B3 shows MRD- NT_{50} . For the others parameters impact of updraft are uncommon.

It appears that updraft tends to impact mainly concentrations of small hydrometeors and IWC for some type of MCS and some MCS reflectivity zones. So for NT (Figure B2), we observe larger NT for updraft in MCS observed over Cayenne, Maldives and Niamey. For Cayenne, it appears in MCS reflectivity zone 5 and 6 for temperatures between 245K and 265 K with NT 2 to 3 times larger than NT for merged dataset. For MCS over Maldives, median NT are 5 times to 20 times larger than NT when there is no noticeable vertical movement in MCS reflectivity zones 6, 7 and 8. Finally for MCS over Niamey, we observe larger NT in updraft than NT for the merged dataset in MCS reflectivity zones 6 for T around 240 K and in MCS reflectivity zones 8 above the bright band. We have similar conclusions for NT_{50} (Figure B3), except that ratios between NT_{50} in updraft and NT_{50} when no updraft is smaller than the ratio between NT in updraft and NT when no updraft.

IWC are impacted by updraft, only for MCS over Cayenne, in MCS reflectivity zone 4, 5, 6 and 7. IWC in updraft tend to be larger about +50% than IWC when no updraft, except in MCS reflectivity zones where IWC are about 2 times larger in updraft than IWC when no updraft.

This investigation on the impact of updraft and downdraft on ice microphysics, shows that updraft may have an impact on concentrations of small hydrometeors and IWC. However, updraft does not impact all type of MCS in the same way. So, there will need to perform deeper investigations on updraft impact.

Despite some noticeable impact of updraft on ice microphysic for our dataset, there is no significant (recurrence trough all types of MCS or as function of T or Z) results to assess them for the merged dataset. So, the parameterization provided in the next section are not functions of vertical velocity.

6. Parameterizations as function of IWC and T

6.1 visible extinction

Since we concluded from Figure 7 and Figure 8 that visible extinction σ and IWC in tropical MCS tend to be similar for all MCS locations in the same range of T and for corresponding MCS reflectivity zones 4 to 8. Moreover Figure 19 shows that there is a linear relationship between $\log(\sigma)$ and $\log(IWC)$. Moreover it seems that $\log(\sigma)$ decrease with temperature increasing at constant $\log(IWC)$. Then, we performed a surface fitting using input coefficients $\log(IWC)$ and T to fit $\log(\sigma)$ to deduce a parametrization of σ (Eq. (8)) as a function of IWC and T for deep convective cloud data (merged dataset) of this study limiting data to $IWC > 0.1\text{g m}^{-3}$:

$$\sigma = \exp(-0.0194587 \cdot T + 0.9134019 \cdot \ln(IWC) + 1.2423609) \quad [m^{-1}] \quad (8)$$

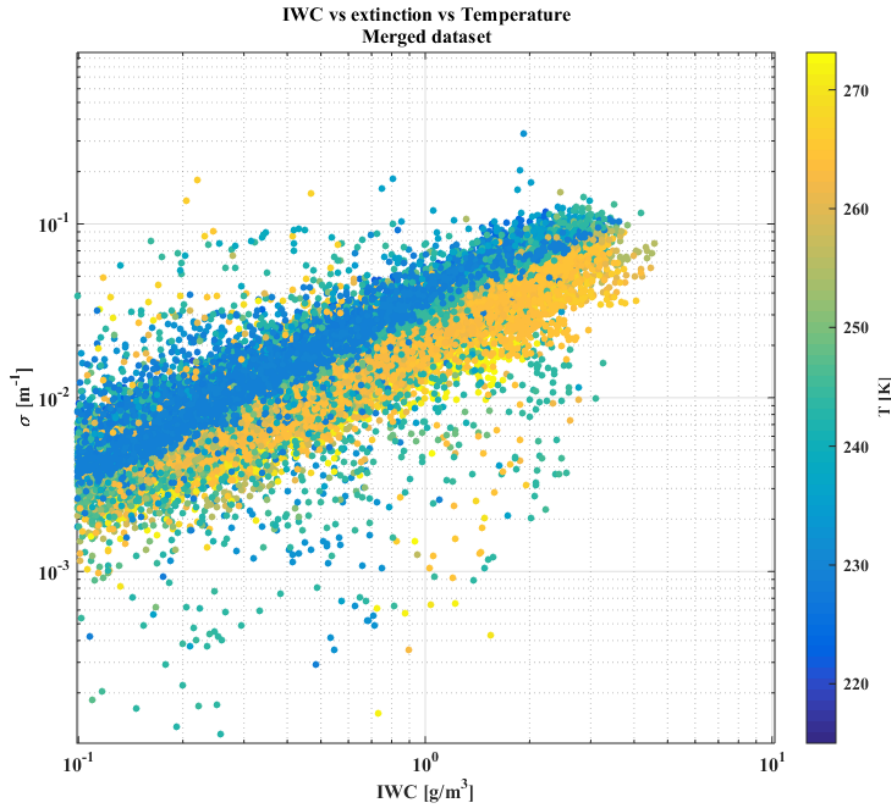


Figure 19: visible extinction in $[m^{-1}]$ on y-axis as function of IWC in $[kg.m^{-3}]$ on x axis and as function of T in $[K]$ with color scale. Scatter plot using the merged dataset (4 campaigns).

An evaluation of this parametrization is presented in Figure 20, where black lines in Figure 20-a) to Figure 20-d) represent median relative errors of σ (with 25th and 75th percentiles represented by whiskers) for the merged dataset predicted with Eq. (8) with respect to retrieved σ from OAP images from Eq. (2). In addition, median relative errors of σ for individual MCS datasets over Darwin, Cayenne, Maldives Islands, and Niamey with respect to σ calculations (Eq. (8)) are shown in Figure 20(a), Figure 20(b), Figure 20(c), and Figure 20(d), respectively. The uncertainty $\pm \frac{U(\sigma)}{\sigma}$ is given with the grey band. All relative errors (25th - 75th percentiles) tend to be smaller than $\pm \frac{U(\sigma)}{\sigma}$, with median relative errors that are smaller than $\pm 25\%$ of σ uncertainty calculated from Eq. (2). In general, Eq. (8) seems to produce smallest relative errors of σ for Niamey and Darwin datasets (especially for $IWC < 2g m^{-3}$).

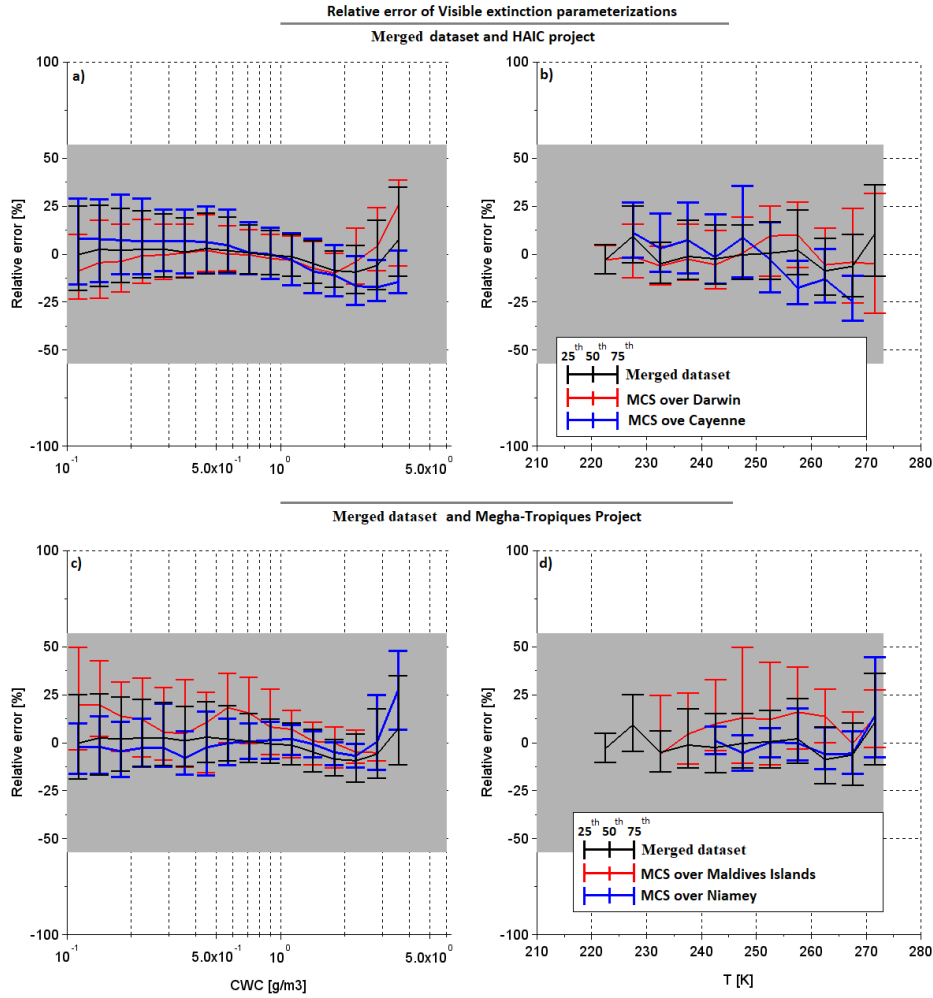


Figure 20: Relative errors of predicted visible extinction Eq. (3) with respect to measured visible extinction for a), b), c), and d). Relative errors as a function of IWC in a) and c) and as a function of T in b) and d). Black lines in 4 sub figures represent the relative errors when calculated for the entire tropical dataset. In a) and b) red lines show median relative error for MCS over Darwin, and blue line for MCS over Cayenne. In c) and d) red line represent median relative errors for MCS over Maldives Islands and blue lines for MCS over Niamey. Bottom of error bar shows 25th percentiles of relative errors and 75th percentiles are given by top of error bar.

To sum up, visible extinction calculated from equation (1) showed similar behavior for all four types of tropical MCS. Indeed, for the same range of temperature and radar reflectivity factors we find very comparable visible extinction in all 4 MCS locations, thereby taking into account the measurement uncertainty. Similar results as for the visible extinction has been documented in a previous section for IWC. From those two results, we can assume that in MCS zones where IWC is larger than 0.1 g m^{-3} hydrometeor populations are similar in shape and density. This is why the development of a parameterization of the visible extinction as a function of temperature and IWC (beyond 0.1 g m^{-3}) has been presented (see equation (3)). Noteworthy, optically thick clouds are responsible of large errors in retrieved cloud water path and condensed water concentration profiles retrieved from satellite imageries (Smith, 2014; Yost et al., 2010). Parameterizations, such as presented here, could help to improve retrieval methods on cloud water path but more investigations on the benefit of such parameterizations are needed, which is beyond the scope of this study.

6.2 Parameterization of ice hydrometeors distributions

6.2.1 Observations of PSD moment

Moments of PSD are convenient for numerical weather prediction to model microphysics of hydrometeor populations, since knowing the PSD n^{th} order moment allows to roughly describe cloud processes and their hydrometeors properties. Commonly, PSD of ice hydrometeors are modeled with Gamma distributions

(Heymsfield et al., 2013; McFarquhar et al., 2007). The calculation of the n^{th} order moment is defined in Eq. (9) for PSD obtained from size distribution measurements of hydrometeors, for example with OAP (optical array probes):

$$M_n = \sum_{D_{\max}=55\mu\text{m}}^{D_{\max}=1,2\text{cm}} N(D_{\max}) \cdot D_{\max}^n \cdot \Delta D_{\max} \quad [m^{n-3}] \quad (9)$$

The uncertainty of the n^{th} ($n=2$ and 3 in our study) moment is:

$$\frac{U(M_n)}{M_n} = \sqrt{n \cdot \frac{U(D)^2}{D} + \frac{U(N)^2}{N}} \quad (10)$$

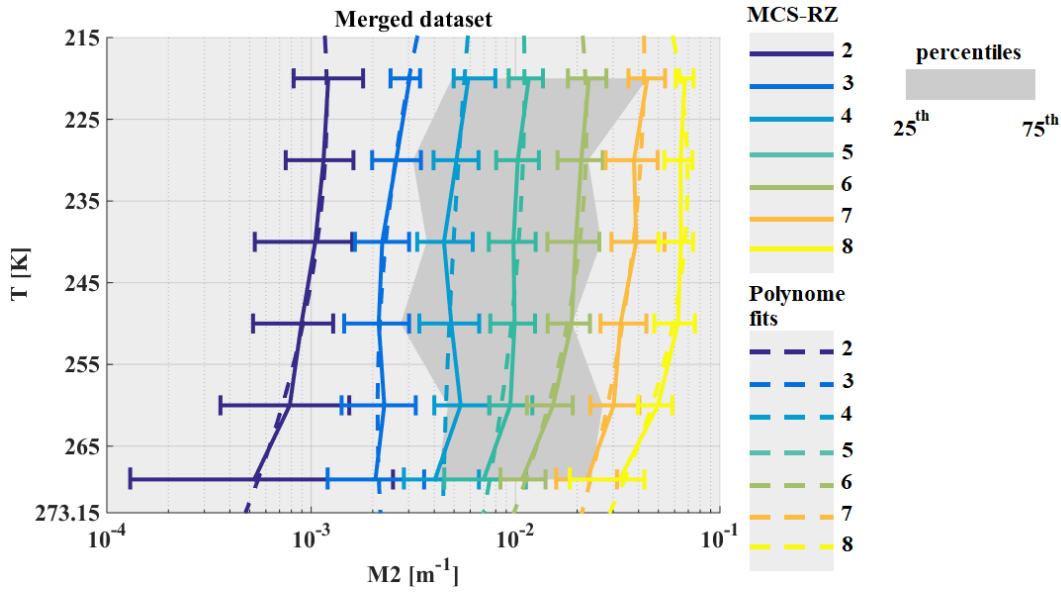


Figure 21: Same as Figure 5, but for M_2 per meter.

Figure 21 shows median second moment M_2 as a function of T for all MCS reflectivity zones for the merged global tropical dataset. Median M_2 slightly decrease with temperature for all individual MCS reflectivity zones, and distinctly increase with MCS reflectivity zone for a given T . The range of variability of median M_2 shows mainly negligible overlap, if any, of 25th and 75th percentiles of neighboring MCS reflectivity zones with the exception between MCS reflectivity zones 8 and 7 at low altitude ($T \in [265; 273.15]$).

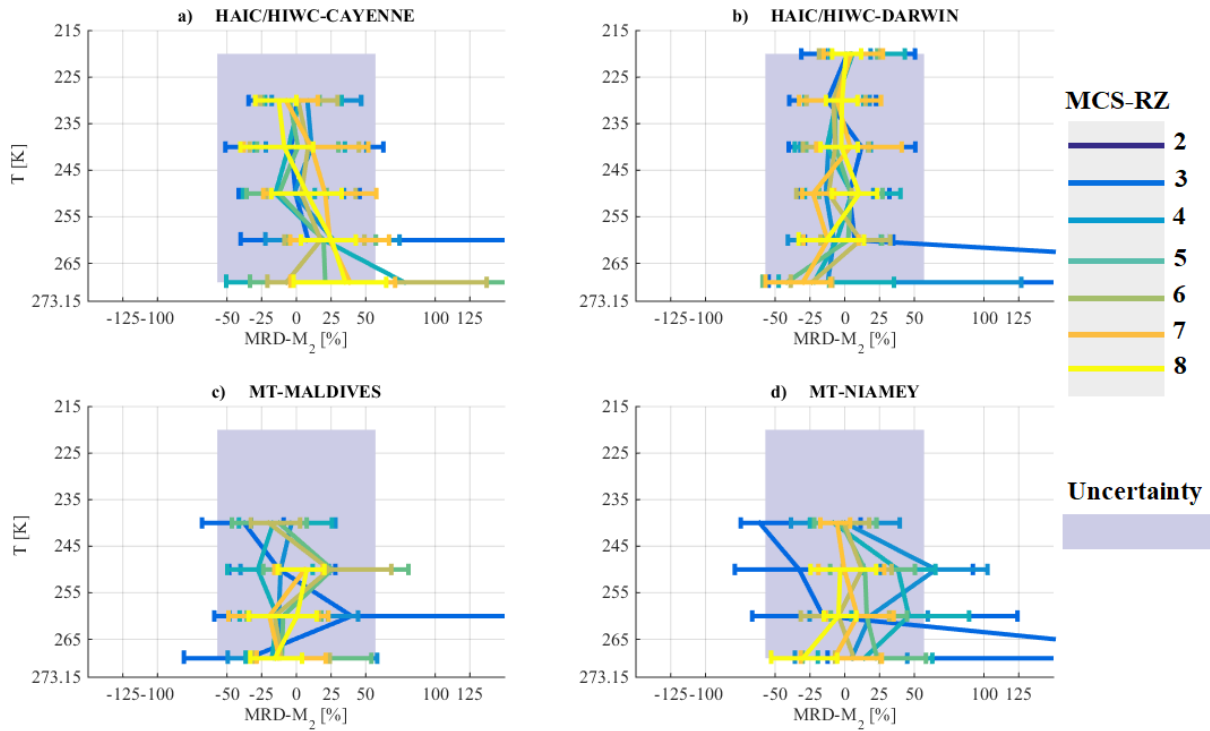


Figure 22: Same as Figure 6, but for MRD- M_2 .

All 4 tropical MCS (Figure 22 (a), (b), (c), and (d)) show good agreement with the medians of M_2 in MCS reflectivity zones 3 to 8, with MRD- M_2 significantly smaller than $U(M_2)/M_2$. Few minor exceptions can be found for MCS over Cayenne (Figure 22 (b)) and Darwin (Figure 22 (c)) in the temperature range [265K; 273.15]. Also MCS over Niamey (Figure 22 (e)) show a larger MRD- M_2 in MCS reflectivity zones 2 and 3 for $T \in [265K; 273.15K]$ and $T \in [245K; 255K]$, respectively.

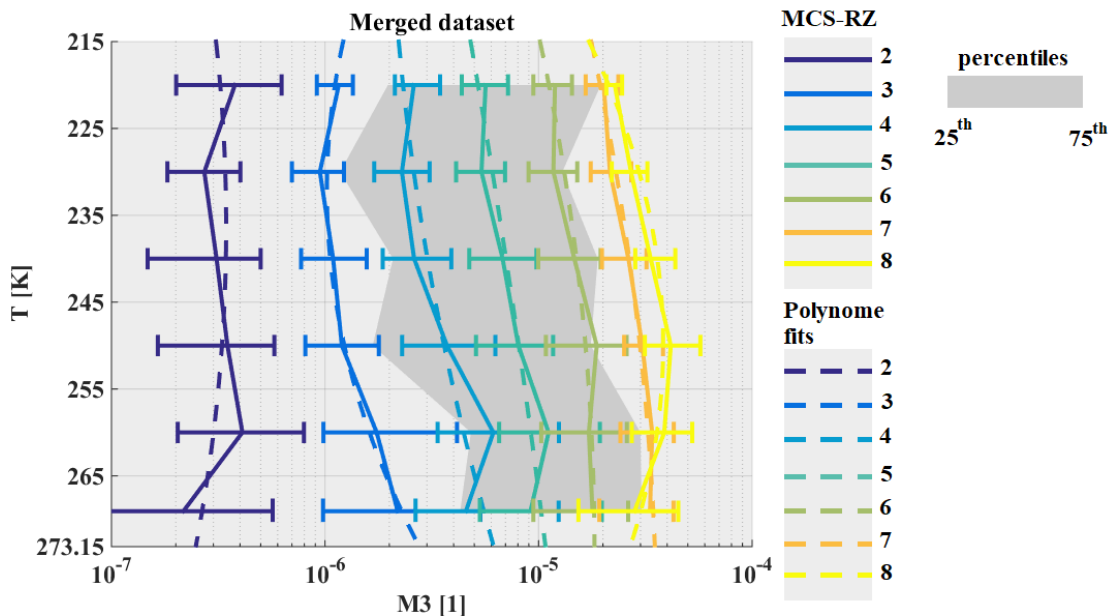


Figure 23: Same as Figure 5, but for the M_3 for unity dimension.

Figure 23 presents median third moment M_3 for global tropical dataset as a function of T and for different MCS reflectivity zones. Median M_3 in highest MCS reflectivity zones 8, 7, and to some extent zone 6 resemble the corresponding curves of median IWC (Figure 5), with a maximum value for median M_3 for $T \in [245K; 260K]$. We also obtain a clear increase in median M_3 with MCS reflectivity zone from 2 to 8. The range of variability for M_3

reveals no overlap of 25th and 75th percentiles of neighboring MCS reflectivity zones 2-7, solely zone 7 overlaps with zone 8 for all temperatures. Third moment of MCS over Cayenne, Darwin and Maldives Islands in MCS reflectivity zones 2 to 8, shows $MRD-M_3$ smaller than $U(M_3)/M_3$, with few minor exceptions basically in the range of $T \in [265K; 273.15K]$. MCS over Niamey tend to have $MRD-M_3$ that are sometimes larger than $U(M_3)/M_3$. Indeed, M_3 for MCS over Niamey tend to be larger in MCS reflectivity zones 5 and 2 in the range of $T \in [265K; 273.15K]$, and in MCS reflectivity zone 4 for T larger than 255K as well as in MCS reflectivity zone 3 for T larger than 245K.

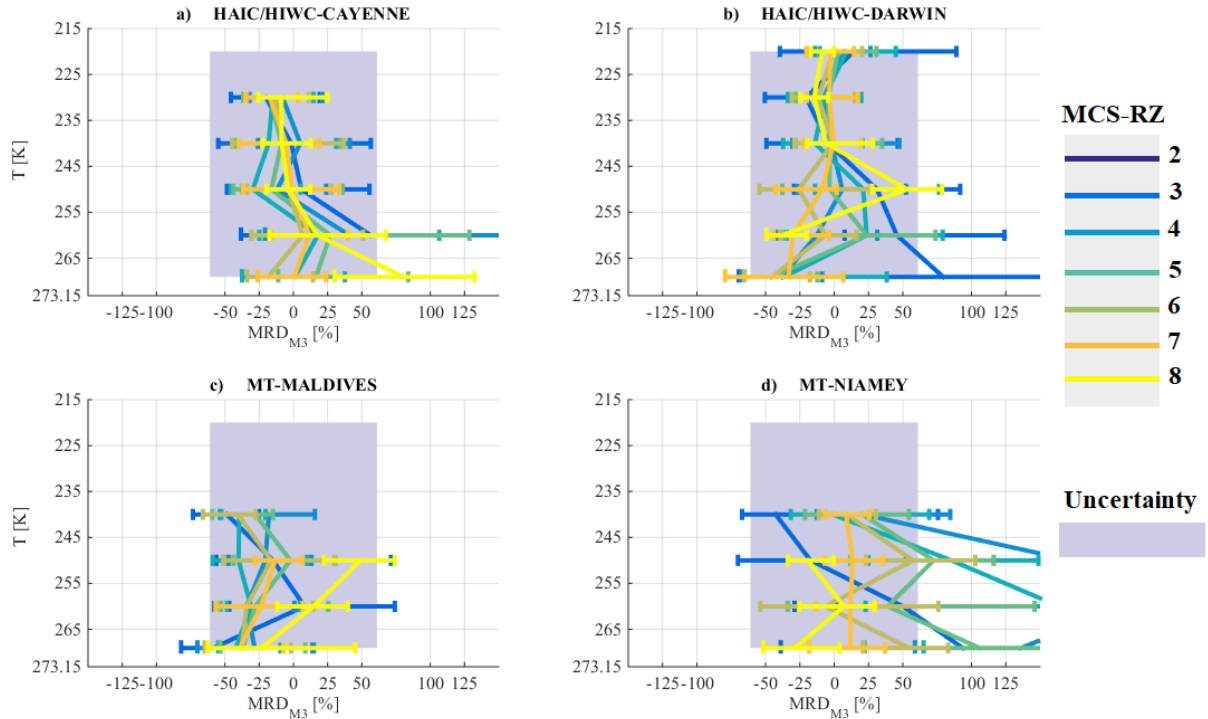


Figure 24: Same as Figure 6, but for the M_3 .

Overall, this section illustrates that second and third moments of PSD are similar as a function of T and Z for all MCS locations of the underlying dataset. However, there are exceptions in MCS reflectivity zones 2, 3 and 4 in MCS over Niamey where larger third moments are calculated compared to those deduced for the merged global tropical dataset. Despite those exceptions, the next section explores the possibility to parameterize the second and third PSD moments as a function of IWC and temperature.

6.2.2 Parameterizations of M_2 and M_3

This section presents parametrizations to predict the 2nd and 3rd moment of the PSD for the merged dataset as a function of T and IWC (for this section IWC in the equation are in $[kg m^{-3}]$), including IWC data larger than $0.1g m^{-3}$. Indeed some moments can be directly linked to bulk properties of hydrometeor populations. For example, moment M_0 for ice and liquid hydrometeors is equal to the total number concentration (N_T), moments M_2 and M_3 for liquid particles are proportional to visible extinction and liquid water content. However, for ice hydrometeors the physical interpretation of moments M_2 and M_3 is less obvious since ice hydrometeors are not spherical particles. The results for α and β coefficients of the $m(D_{max})$ relationship presented in section 5.3, illustrate that β varies between 1.5 and 2.3. This means that IWC is proportional to PSD moments between $M_{1.5}$ and $M_{2.3}$. Also uncertainties on the retrieved β coefficients do not allow to assess the variability of β as a function of IWC and T . Former studies performed in different cloud environments report mean values of β around 2. For example, Leroy et al., (2016) found $\beta=2.15$ for HAIC-HIWC in Darwin, Cotton et al., (2013) suggested $\beta=2.0$, Heymsfield et al., (2010) suggested $\beta=2.1$, and Brown and Francis (1995) established $\beta=1.9$. We are also aware of the fact that findings of β also depend on the utilized size parameter (D_{max} , D_{eq} , etc...) of 2D images. Hence, we apply $\beta=2$ as

an approximation, also proposed by Field et al., (2007), to link the second moment of hydrometeor PSD with IWC (Eq. 11). Subsequently the ratio IWC/M_2 is calculated and denoted A.

$$M_2 = \frac{IWC}{A} \quad [m^{-1}] \quad (11)$$

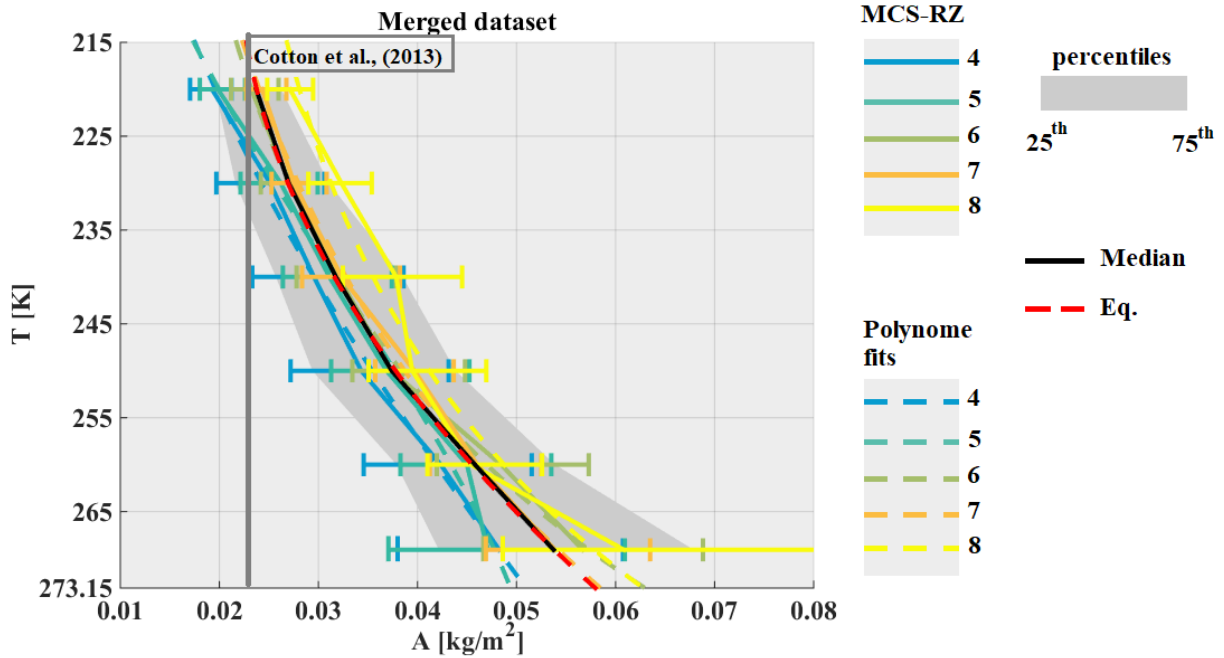


Figure 25: Same as Figure 5, but for the ratio $A = IWC/M_2$ in $[kg\ m^{-2}]$.

Figure 25 shows retrieved median coefficients A for the global tropical dataset as a function of MCS reflectivity zone and T. Note that A is calculated in SI units (note that in Eq. (11) IWC is in $kg\ m^{-3}$). The black solid line gives the median of A as a function of T, thereby merging all MCS reflectivity zones for the merged dataset with $IWC > 0.1g\ m^{-3}$. The grey band gives corresponding 25th and 75th percentiles of that median A. In addition, are calculated median A for all individual MCS reflectivity zones (on Figure 25) are solely illustrated median A for zones 4 to 8) for the global tropical dataset as a function of T. In general, median A calculated for individual MCS reflectivity zones 5, 6 and 7 are very similar to the median A when merging all MCS reflectivity zones (black solid line), whereas median A calculated for MCS reflectivity zone 4 tends to have smaller A values and median A calculated for MCS reflectivity zone 8 have larger median A values than the overall median A (all MCS reflectivity zones merged) for comparable temperatures.

However, when taking into account the variability in median A calculated for individual MCS reflectivity zones and associated 25th and 75th percentiles we can state that median A generally increases with T, however it is not possible to assess that A increases with MCS reflectivity zones or IWC. As a comparison, we include the value of the pre-factor α (in SI unity) from Cotton et al. (2013) mass-size relationship ($\beta=2.0$, as is for second moment M_2 , and $\alpha=0.0257$). Clearly, $\alpha=0.0257$ is not suited for deep convective systems as it represents ice crystals for $T \in [215K; 225K]$.

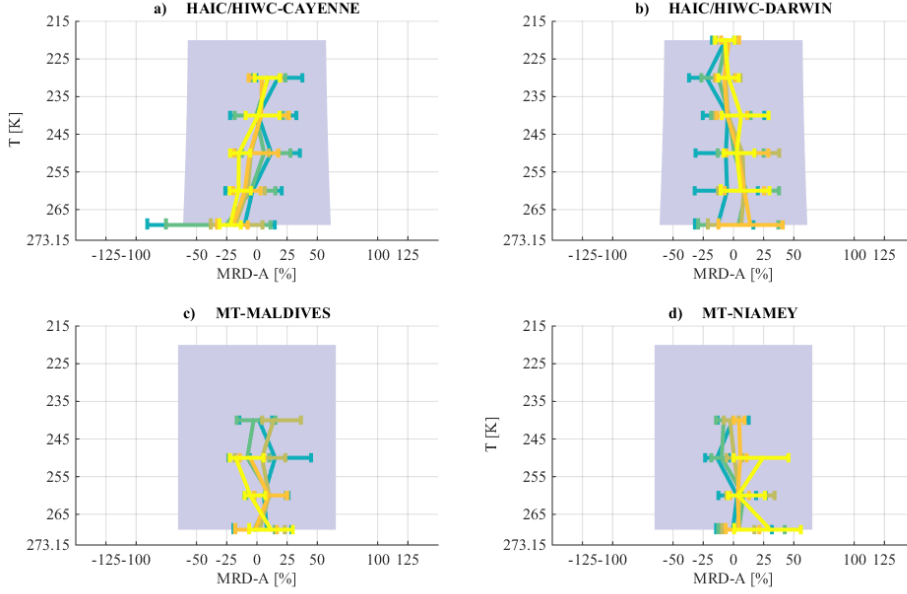


Figure 26: Same as Figure 6, but for the ratio MRD-A.

Figure 26 (a), 26(b), 26(c), and 26(d) illustrate that MRD-A are significantly smaller than $U(A)/A$, (same uncertainty than α : $U(\alpha)/\alpha = U(A)/A$ and median MRD results centered around 0%). Comparing results of A (Figure 26) with results presented for α (Figure 15, section 5.4) it is obvious in terms of variability and MRD in each type of MCS that A is better adapted to parametrize the PSD 2nd moment as a function of T . Eq. (12) then fits the median of ratio A for the global tropical dataset (red dashed line, all MCS reflectivity zones merged), as a function of T in deep convective systems for IWC larger $0.1g\ m^{-3}$:

$$A(T) = 0.0000075 \cdot T^2 - 0.0030598 \cdot T + 0.3334963 \quad [kg \cdot m^{-2}] \quad (12)$$

Hence, Field et al., (2007) proposed to retrieve the third moment M_3 as function of M_2 and T . These equations are recalled here with (in our case $n=3$):

$$M_n = M_2^{F(n)} \cdot D(n) \cdot \exp(E(n) \cdot T_c) \quad (13)$$

T_c denotes temperature in °C and $D(n)$, $E(n)$ and $F(n)$ are given by:

$$D(n) = \exp(13.6 - 7.76 \cdot n + 0.479 \cdot n^2) \quad (14)$$

$$E(n) = -0.0361 + 0.0151 \cdot n + 0.00149 \cdot n^2 \quad (15)$$

$$F(n) = 0.807 + 0.00581 \cdot n + 0.0457 \cdot n^2 \quad (16)$$

Figure 27 provides median relative errors (whiskers represent 25th and 75th percentiles) of parametrized moments M_2 (Figure 27 (a) and Figure 27 (b)) and M_3 (Figure 27 (c) and Figure 27 (d)) compared to respective moments calculated directly (Eq. (9) from PSD measurements (merged dataset)). These relative errors are shown as a function of IWC (Figure 27(a) and Figure 27(c)) and as a function of T (Figure 27(b) and Figure 27(d)). Firstly, the red line shows median relative error of M_2 retrieved from Eq. (11) compared to M_2 derived from measured PSD (Eq. (10)). In addition the grey band illustrates the uncertainty $U(M_2)/M_2$. Figure 27 (a) illustrates that below $2g\ m^{-3}$, the median of this relative error is close to 0% with 25th and 75th percentiles significantly smaller than $U(M_2)/M_2$. However, for largest IWC beyond $2g\ m^{-3}$, median relative errors are getting large (40% for $4g\ m^{-3}$ and 75% for $4.5g\ m^{-3}$) and need to be corrected in order to reduce the bias between predicted M_2 and observed M_2 . This is why Eq. (11) is modified with an expression shown in Eq. (17) in order to improve prediction of M_2 compared to measured M_2 (Eq. (10)) for highest IWC:

$$M_2 = \frac{IWC}{A(T)} \cdot \exp(0.005853 \cdot \exp(1025 \cdot IWC)) \quad [m^{-1}] \quad (17)$$

The effect of the expression added in Eq. (17) is illustrated by the blue line in Figure 27 (a) and Figure 27 (b), where median relative error of predicted M_2 are now closer to 0% also for large IWC. ~~Still, Eq. (12+17) seems to underestimate measured M_2 by about 15% for IWC of 4.5 g m^{-3} instead of 75% overestimation before correction.~~ Note that in Figure 27 (b), median relative errors of the two above parametrizations (red and blue solid line) of M_2 are superposed as a function of T with a median relative error close to 0%. This means that the second part of equation (17) does not introduce any significant bias as a function of T , since the occurrence of $\text{IWC} > 2 \text{ g m}^{-3}$ is smaller than 1% for the merged dataset.

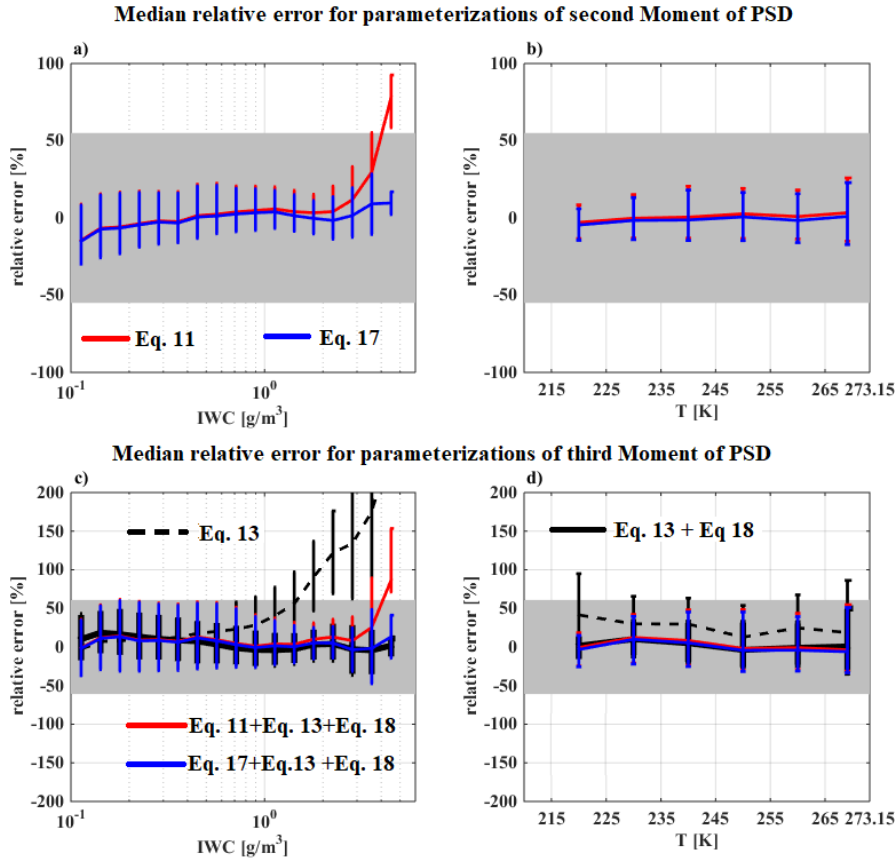


Figure 27: Relative error of parametrized M_2 and M_3 for merged dataset as a function of IWC in a) and c), and as a function of T in b) and d). Solid lines give median relative error and whiskers denote 25th and 75th percentiles of relative error. Grey bands shows measurement uncertainties for M_2 (55%; a) and b)) and M_3 (61%; c) and d)), respectively.

In Figure 27 (c) and Figure 27 (d) are shown median relative error for parameterizations of the third moment, where the median relative error for all parameterization are calculated as function of measured M_3 . First, we discuss the median relative error for parametrization of 3rd moment M_3 according to Field et al., (2007) (Eq. (13); black dashed lines) using the measured M_2 . Then, we can see that the parameterization of Field et al., (2007) overestimate M_3 for IWC larger than 1 g m^{-3} and that overestimation of M_3 increase with IWC. Moreover, this overestimation of M_3 tend to decrease a bit as function of T .

To reduce this significant median relative error on measured M_3 , particularly for large IWC in deep convective cloud systems, we provide a M_3 correction function for Eq. (13) as function of T and IWC:

$$M_3 = [-5.605 - 1.059 \cdot \log(\text{IWC}) + 0.009536 \cdot T - 0.0418 \cdot \log(\text{IWC})^2 + 0.0007889 \cdot \log(\text{IWC}) \cdot T] \cdot M_2^{F(3)} \cdot D(3) \cdot \exp(E(3) \cdot T_c) \quad (18)$$

Then, three series of median relative error of M_3 where M_3 are computed with Eq. (19). First, Eq. (19) is used with measured M_2 (black solid lines) to show the efficiency of the correction applied as function of IWC and T and described in Eq. (19). Then, Eq. (19) is applied to M_2 calculated using Eq. (11) where there is no correction as function of IWC to calculate M_2 (red solid lines). We can observe that M_3 are overestimated for IWC larger than

3g.m-3, and that there is no bias as function of T with median relative error close to 0%. Finally, Eq. (19) is used to compute M_3 from M_2 calculated with Eq. (17) when impact of large IWC is taken into account. We can see median relative error close to 0% for the third example of parameterization (i.e. Eq. (17) and Eq. (18)) with no bias as function of IWC and T .

An identical investigation on median relative errors in the prediction of 2nd and 3rd moment as presented in Figure 27 has been investigated for individual MCS locations (figures not shown). For all type of tropical MCS, we observe that M_2 from Eq. (17) and M_3 from Eq. (18) tend to have smaller to equal median relative errors compared to the relative uncertainties $U(M_2)/M_2$ and $U(M_3)/M_3$, respectively. Beyond this general statement there are two noticeable observations. The first observation is that median relative errors of M_3 from Eq. (18) calculated either with M_2 from measurements (Eq. (9)) or from parametrized M_2 from Eq. (17) for MCS over Maldives Islands are close to $U(M_3)/M_3$ with 75th percentiles reaching 100% for IWC in the $[0.3; 0.6] \text{ g m}^{-3}$. The second observation is that for MCS over Niamey, M_3 from Eq. (18) with M_2 from Eq. (9) or from Eq. (17) tend to overestimate respective moments calculated directly from PSD measurements by about 30 or 50%, respectively, in the area of higher IWC ($[2; 3] \text{ g m}^{-3}$).

This section aims to produce parameterizations of the second and third moments of ice hydrometeor size distributions, which can be useful for the calculation of hydrometeor size distributions in numerical weather prediction using gamma distributions, but also (see the next section) for calculating rescaled ice hydrometeors size distributions (Field et al., 2007).

6.2.3 Rescaling of measured ice hydrometeors size distributions

From bulk properties as mixing ratio and total concentration in numerical weather prediction (NWP), ice hydrometeors size distributions (or PSD) properties can be derived from moment parameterization allowing simplified prediction of cloud microphysical processes such as precipitation. Usually, ice hydrometeors size distributions for hydrometeors are modeled by gamma distributions. Since the method of gamma distributions is relatively well documented, we focus this study on another type of PSD parameterization, which studies 'rescaled PSD' dealing with a 'mean diameter' defined by the ratio of the third moment over the second moment.

In this section, we propose an update for the method proposed by Field et al., (2007) for deep convective cloud systems and IWC larger than 0.1 g m^{-3} . For the entire dataset of this study we therefore apply the above method utilizing Eq. (19) and Eq. (20) to calculate function $\Phi_{2,3}(x)$ and x for individual measured PSD :

$$\Phi_{2,3}(x) = N(D_{\max}) \cdot \frac{M_3^3}{M_2^4} \quad (19)$$

With x being the characteristic size:

$$x = D_{\max} \cdot \frac{M_2}{M_3} = \frac{D_{\max}}{L_{2,3}} \quad (20)$$

$\Phi_{2,3}(x)$ and x are dimensionless functions. Moreover, Field et al., (2007) deduced from their dataset, $\Phi_{2,3}(x)$ depending on cloud location; i.e. tropical troposphere or mid-latitude troposphere (here we focus on the equation established for the tropics):

$$\text{Tropics: } \Phi_{2,3}(x) = 152 \cdot \exp(-12.4 \cdot x) + 3.28 \cdot x^{-0.78} \cdot \exp(-1.94 \cdot x) \quad (21)$$

Hence, the variability of PSD in clouds, is not given by $\Phi_{2,3}(x)$ but by the variability of the 2nd and 3rd moments that allow retrieving functions x and $\Phi_{2,3}(x)$. Then, knowing x , $\Phi_{2,3}(x)$, M_2 , and M_3 concentrations of ice hydrometeors can be parameterized such:

$$D_{\max} = x \cdot \frac{M_3}{M_2} \quad (22)$$

and

$$N(D_{\max}) = \Phi_{2,3}(x) \cdot \frac{M_2^4}{M_3^3} \quad (23)$$

Figure 28 shows the probability distribution function (PDF) of observed rescaled PSD in tropical MCS as a function of the x parameter. Thick black line represents $\Phi_{2,3}(x)$ from Field et al., (2007), thin dashed grey line represents median of $\Phi_{2,3}(x)$ for a given range of x , with whiskers showing 25th and 75th percentiles of $\Phi_{2,3}(x)$. The figure illustrates that Eq. (21) from Field et al., (2007) represents rather well $\Phi_{2,3}(x)$ as a function of x in highest PDF region (dark red area) and fits well the median plot for $x \in [0.3; 6]$. However, Field et al., (2007) performed their study for diameter larger than 100 μm while this study calculates rescaled PSD for D_{max} larger than 15 μm for the underlying dataset. Thus, Eq. (21) does not fit median $\Phi_{2,3}(x)$ for x smaller than 0.3. Also for $x > 6$, Eq. (21) decreases too fast compared to the median of $\Phi_{2,3}(x)$ calculated for the global tropical dataset of this study, although Field et al., (2007) considered ice hydrometeors up to 2cm, whilst this study extrapolates PSD until 1.2845cm only. A likely assumption to explain the differences for large $x > 6$ might be that the merged tropical dataset of this study may have measured PSD with largest hydrometeors at a far higher frequency than this was the case for the dataset of Field et al., (2007).

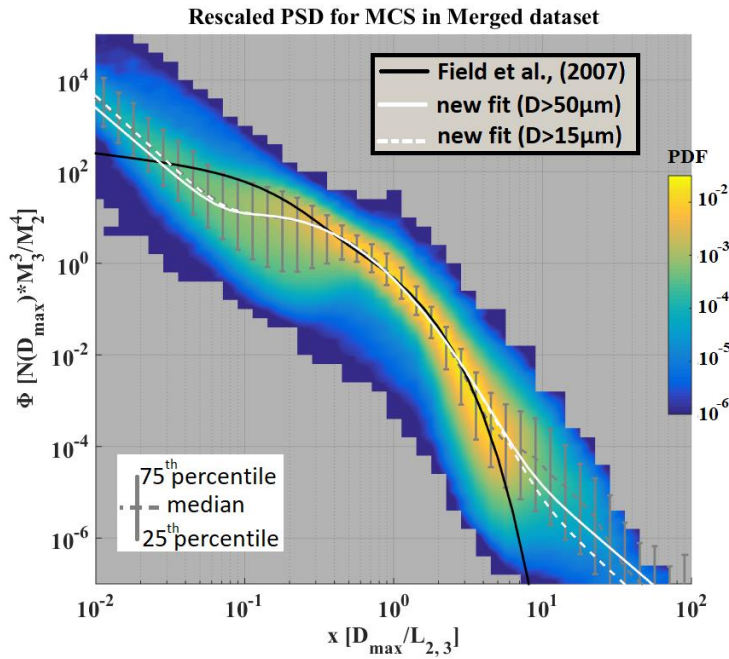


Figure 28: Probability distribution function of rescaled PSD ($\Phi_{2,3}$) on y axis as a function of hydrometeor characteristics size (x) on x axis, for the Global tropical datasets. Black lines show fitted functions from Field et al., (2007), grey dotted lines show median rescaled PSD with error bar from 25th and 75th percentiles of rescaled PSD. Solid white line presents the new fitted function for the global tropical dataset for PSD beyond 55 μm and dashed white line shows fitted function for PSD beyond 15 μm (Eq. 25).

White lines (dashed and solid) show new fitted $\Phi_{2,3}(x)$ for the global tropical dataset of this study. The white dashed and solid lines can be represented by the following equation and aim to fit the median ($\Phi_{2,3}(x)$) of Figure 28 as a function of x :

$$\text{Tropics: } \Phi_{2,3}(x) = [\exp(a_1) \cdot x^{a_2}] + \left[b_1 \cdot \exp\left(-\frac{(\ln(x) - b_2)^2}{b_3^2}\right) \right] \quad (24)$$

Where $b_1 = 9.484$, $b_2 = -1.895$ and $b_3 = 1.083$. Note that dashed and solid white lines use different sets of coefficients a_1 and a_2 (Table 1). For white dashed line, a_1 and a_2 are calculated for D_{max} beyond 15 μm , whereas for white solid line, a_1 and a_2 are calculated for D_{max} beyond 55 μm . We can notice that the function for $D_{\text{max}} \geq 15\mu\text{m}$ produces higher $\Phi_{2,3}(x)$ as compared to the function fitted for $D_{\text{max}} \geq 55\mu\text{m}$. In order to explain this difference, we recall that for MCSs over the Maldives Island concentrations of hydrometeors with $D_{\text{max}} \leq 55\mu\text{m}$ are higher compared to 3 other tropical MCS locations, which could affect the fitted coefficients a_1 and a_2 in the two different versions of $\Phi_{2,3}(x)$ calculations for the global tropical dataset. Another difference in small particle measurements could be a pure technical difference in small particle measurements (including shattering/out-of-focus/small sample volume artefacts) between 2D-S probe (this study) and 2D-C probe (Field et al. (2007) study).

Table 1 : Coefficients a_1 and a_2 for Eq. (25).

	a_1	a_2
Tropics: $D_{max} > 15\mu m$	-5.4114	-3.0026
Tropics: $D_{max} > 55\mu m$	-5.0032	-2.7822

”

Discussion of results:

The discussion would benefit from relating your results to results of former studies, do your findings agree/disagree with what others have found? If your results are completely new, than it should be pointed out more clearly! Also, please point out more clearly what your parameterisations are useful for and how the scientific community benefits from your work.

In section 5.1, we compare our results to IWC-T relationship calculated for clouds in the tropics : “*For comparison purposes with former studies, two IWC-T relationships from literature are added in Figure 5(a). Jensen and Del Genio (2003) suggested an IWC-T relationship in order to account for the limited sensitivity of the precipitation radar aboard the TRMM satellite, not allowing for small ice crystals at the top of convective clouds’ anvils to be observed. They used radar reflectivity factors of a 35GHz radar based on Manus Island (North-East of Australia; 2.058°S, 147.425°E), thereby calculating IWC from an IWC-Z relationship ($IWC=0.5*(0.5.Z^{0.36})$); Jensen et al., 2002). The resulting IWC-T relationship given by Jensen and Del Genio (2003) is reported by a dashed-dotted grey line, which fits between 75th percentiles of tropical median IWC of MCS reflectivity zone 4 and 25th percentile of MCS reflectivity zones 5. We recall that IWC, as a function of T, in MCS reflectivity zones 4 and 5 are related to Z between 30th-50th and 50th-70th percentiles, respectively. We may notice that the IWC-T relationship from Jensen and Del Genio (2003) is different and smaller than the median IWC (4 tropical campaigns). Moreover, (Heymsfield et al., 2009) established an IWC-T relationship based on 7 fields campaigns (dashed grey line in Figure 5(a). They focused their study on maritime updrafts in tropical atmosphere for a temperature range $T \in [213.15K; 253.15K]$. Their suggested IWC tend to be in the range of IWC of MCS reflectivity zones 6- 8 with IWC increasing with T. We already showed in section 3.2 that MCS reflectivity zones 7 and 8 have higher probabilities to be convective (updraft regions with higher magnitudes of vertical velocity), as compared to other MCS reflectivity zones. Therefore, (Heymsfield et al., 2009) IWC parametrizations for maritime updrafts are not inconsistent with data from this study.*”

In section 5.2, we compare our results from visible extinction-T relationships from Heymsfield et al., (2009): “*Furthermore, a σ -T relationship from Heymsfield et al. (2009) (grey dashed line) is added in Figure 6 (a), which is calculated, as a function of T, as the sum of the total area of particles larger than $50\mu m$ plus the total area of particles smaller than $50\mu m$ multiplied with a factor of 2 in order to satisfy Eq. (1) and to compare with results of this study. We conclude that σ -T estimation presented in Heymsfield et al. (2009) for maritime convective clouds is rather comparable to median MRD- σ calculations (4 tropical campaigns) in MCS reflectivity zones 6 to 7 corresponding to higher reflectivity zones, and thus statistically to zones with some remaining convective strength.*”

Page 18 line 9, we propose to add references who founds similar results (R2#5).

“*It confirms conclusions from Frey et al., (2011) and Cetrone and Houze (2009), who suggest that there are larger ice hydrometeors in MCS over continent than MCS over maritime regions.*”

Also, we performed an update and a comparison of parameterization of 2nd Moment and 3rd Moment of PSD and the parameterization of ice hydrometeors size distribution as function of IWC and T performed by Field et al., 2007 for tropical convective clouds. This parameterization was used in the microphysical scheme based on (Wilson and Ballard, 1999) used in the configuration of the Met Office Global Atmosphere version 6.1 (Walters et al., 2017). Which was the version of the Unified Model used operationally by the Met Office for global weather and climate prediction. More precisely, the ice-snow concentrations was computed with the moment parametrization developed by (Field et al., 2007) and the mass-diameter relationship from Cotton et al., (2013).

We propose to add the following comment in the conclusion section at the page 28 line 8 of the original version of the manuscript (R2#6):

“*To conclude on the parameterization of ice hydrometeors distribution. We performed an update of the computation of PSD as function of IWC and T performed by Field et al., 2007 for tropical convective clouds (see*

Eq. (11), Eq. (17) and Eq. (18)). This parameterization was used in the microphysical scheme based on (Wilson and Ballard, 1999) used in the configuration of the Met Office Global Atmosphere version 6.1 (Walters et al., 2017). Which was the version of the Unified Model used operationally by the Met Office for global weather and climate prediction. More precisely, the ice-snow concentrations was computed with the moment parameterization developed by (Field et al., 2007) and the mass-diameter relationship from Cotton et al., (2013). Here, we suggest to use the new parameterization developed in our study for ice-snow concentrations when IWC are larger than 0.1 g.m^{-3} . Otherwise, we suggest to keep either the original version of Field et al., (2007) parameterization with the Cotton et al., (2013) mass size relationship or the original version of Field et al., (2007) parameterization with A as function of temperature which would be a fit of the 25th percentile of A in MCS reflectivity zone 4 (see Table C12 in Appendices C).”

Moreover, we propose to add a comment on how to use the MCS reflectivity zones after the former comment (R2#7).

“We showed that IWC tend to be similar as function of temperature and MCS reflectivity zone, suggesting that IWC-Z-T relationship developed by Protat et al., (2016) would be available for IWC larger than 0.1 g.m^{-3} in tropical MCS. In other words there is a confident relationship between IWC, Z and T in tropical MCS. Then, for the evaluation of NWP, we suggest to define the MCS reflectivity zones using the 25th percentiles of IWC as the lower limit of each MCS reflectivity zones (see Table C2 in Appendices C). Hence, for each MCS reflectivity zone visible extinction, hydrometeors concentrations (NT_{50} , NT_{500} , M_2 and M_3), reflectivity factors at 94GHz and vertical velocities from NWP can be compared with the findings of this study (see Table in Appendices C). This methodology should help to identify where NWP fails to represent the links between different parameters and IWC. Indeed, study the spatiotemporal variability of IWC in MCS is a complex topic. It needs a time reference and a space reference. For MCS, the time reference can be its life cycle, but there are MCS that have a more complex life cycle than others (merging of MCS, a new growing stage after a decaying stage). Concerning the space reference, there is a common view which is to observe the MCS from its most active area; its convective part. There are two difficulties to take into account here. First, there are very few direct measurement of cloud microphysic in the very convective area of MCS. Second, MCS can be the aggregation of many convective cells that can be well or not well organized (Houze 2004). Moreover, we saw that large IWC tend to be more associated to vertical movement than lower IWC, but it is not always true. This is why we propose to test NWP using the statistic performed in this study, by testing the different conditions of others microphysical parameters observed with a given IWC and temperature.”

Specific comments

page 2, line 4-5: “An accurate estimation of the spatiotemporal distribution of the Ice Water Content (IWC) is a key 5 parameter for evaluating and improving numerical weather prediction (Stephens et al., 2002).” Does this statement make sense in the light of your manuscript where you use IWC as input for your parameterisation and not obtain it as output?

It is right that IWC in our study is used as an input. In fact, we use it at a key parameter, that will test if the others parameters are in agreement with the range that they are observed knowing IWC and the temperature. See the text added in the end of the former comment.

page 3, line 2: better say: This study uses a data set where MCSs were observed in four different locations in the tropics and related to two different projects:

Done.

page 3, line 19: IKP-2 - please introduce abbreviation.

Change are made in the manuscript such (R2#8):

“performed with the isokinetic evaporator probe (hereafter IKP-2 probe)”

page 3, line 22: Are you really giving D_{max} in cm?

Yes, shape properties of ice crystals are calculated in cgs unit, such mass-size relationship, surface-size relationship and perimeter size relationship. Also note that in section 5.5 largest size of hydrometeors are given in cm.

page 3, line 31: Please introduce the radar reflectivity factor Z as it is an important parameter in your study and reader less familiar with radar measurements might not properly know it.

The definition is introduced at page 2 line 28: “The latter will be accomplished by a composite analyses of microphysical properties and simultaneously measured radar reflectivity factor (Z).”!

page 3, line 35: “The processing holds particularly for both data sets of the HAIC-HIWC project.”

I don’t quite understand what you want to say with this sentence? Please rephrase.

(R2#9)

“Detailed description of data processing is documented in Leroy et al. (2016 and 2017), Protat et al. (2016), Strapp et al. (2016b), and Davison et al. (2016). These references give a processing description for both datasets of the HAIC-HIWC project. But, Megha-Tropiques datasets (Fontaine et al. (2014)) were reprocessed in order to undergo exactly the same version of processing tools for comparison reasons in this study.”

page 4, line 2/3: mean profiles of Z:

Did you perform some kind of weighting when combining the data sets from the four campaigns for the number of data points that go into the mean? If not the results/means will be shifted towards the HAIC-HIWC campaigns, which have significantly more data points. This should be discussed.

We do not use mean profiles, but percentiles profiles. However, percentiles calculation from radar data takes into account more data from cloud radar profiles than for the in-situ data. There are less in-situ measurement for MT project than for cloud radar profiles measurement, because the PIP probe was not working in the second half of the two campaigns of MT project. However, the cloud radar worked perfectly over all the MT-project. The percentiles of Z are calculated for a merged dataset that include 11 flights for MT over Niamey, 11 flights for MT over Maldives, 19 flights for HAIC-HIWC over Darwin and 17 flights for HAIC-HIWC over Cayenne.

We propose to add line 41 page 3 (R2#10):

“The percentiles of Z are calculated for a merged dataset that include 11 flights for MT over Niamey, 11 flights for MT over Maldives, 19 flights for HAIC-HIWC over Darwin and 17 flights for HAIC-HIWC over Cayenne. Percentiles are not calculated as function of the number of profiles but by temperature ranges of 5K where only points with Z larger than -30dBZ are taken into account.”

page 5, line 26: The usage of ECMWF reanalysis temperatures: Due to the much coarser resolution of the ECMWF data (compared to aircraft point measurements), what implications does it have on the uncertainties of your results?

First, profiles are measured as function of their altitude. Then, using reanalysis of ECMWF and knowing the flight altitude and its temperature of the aircraft, the cloud radar profiles temperature is computed. Hence, ECMWF temperature profiles are adjusted for each profiles measured by RASTA by the in-situ measurement of the temperature. So uncertainty of ECMWF reanalysis, affect the statistics on Z profiles as function of the temperature, but it does not affect the statistic on the in-situ measurement.

page 7, line 20f: $U(X)/X$ - Is this parameter denoted by the grey shading in the subfigures b-e? Then mention it here as well.

(R2#11)

“In order to take into account the uncertainties in all type of measurements, uncertainties (hereafter noted $U(X)/X$) represented by grey bands on Figure showing MRD-X) for each parameter X were taken from Baumgardner et al. (2017)”

page 11, line 1-5: You are concluding that “... _ in tropical MCS tend to be similar for all MCS locations in the same range of T and for corresponding MCS reflectivity zones, ...” but your parametrisation is only a function of T and IWC, but not dependent on reflectivity zone? How does that fit? In that respect I was missing a figure showing measured values alongside the parametrisation (not only the relative errors as in Fig. 7). It could also help to explain more how you arrive at this parameterisation.

In section, 5.1 we pointed out that there could be a unique IWC-Z-T relationships (given by Protat et., 2016) for tropical MCS for IWC larger than 0.1g.m-3. So performing a parameterization as function of IWC and T is similar to perform a parameterization as function of reflectivity zones (i.e. Z(T)). A parameterization as function of IWC and T is more convenient than a parameterization as function of Z and T. In the first case, it can be used by model and observations. While in the second case it can only being used with observations, since simulations of radar reflectivity factors at 94 GHz are not accurate for NWP.

When plotting visible extinction versus IWC and T there is a linear relationship between $\log(\sigma)$ and $\log(\text{IWC})$. Moreover it seems that $\log(\sigma)$ decrease with temperature increasing at constant $\log(\text{IWC})$. Then, we performed a surface fitting using input coefficients $\log(\text{IWC})$ and T to fit $\log(\sigma)$.

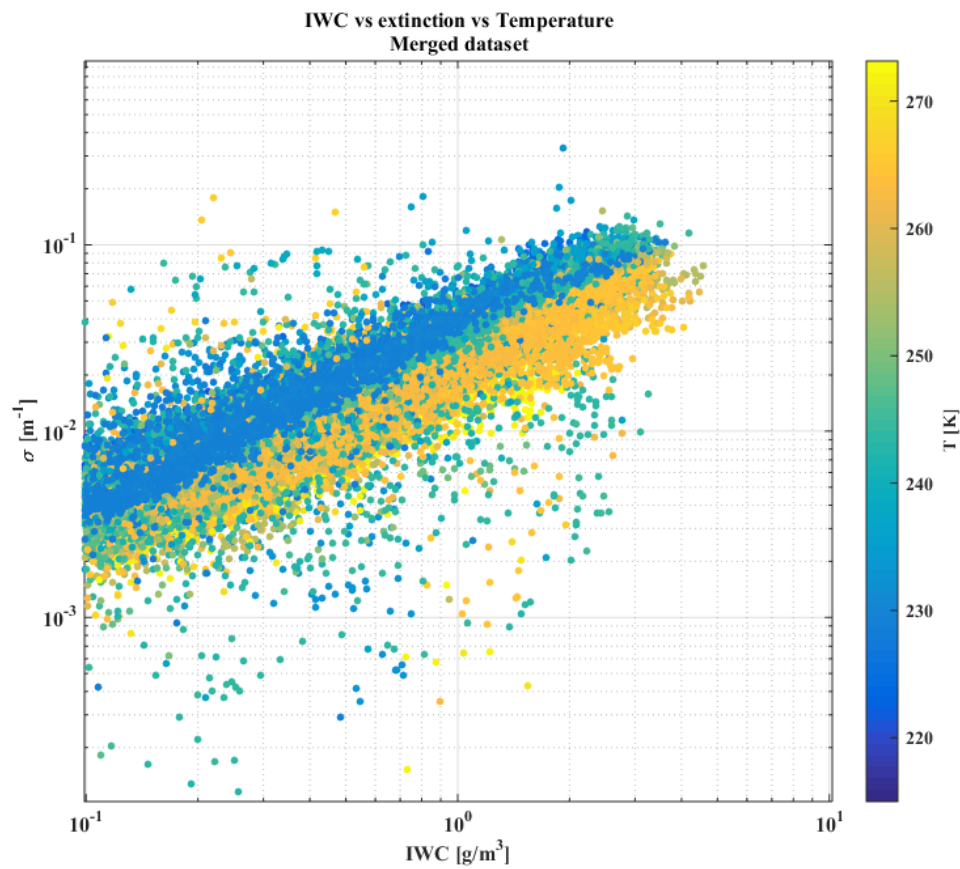


Figure 19: visible extinction in m^{-1} on y-axis as function of IWC in $\text{kg}\cdot\text{m}^{-3}$ on x axis and as function of T in [K] with color scale. Scatter plot using the merged dataset (4 campaigns).

We add the previous figure in the section concerned by parameterization of visible extinction (R2#12; see also answer to the major comment about length of section5).

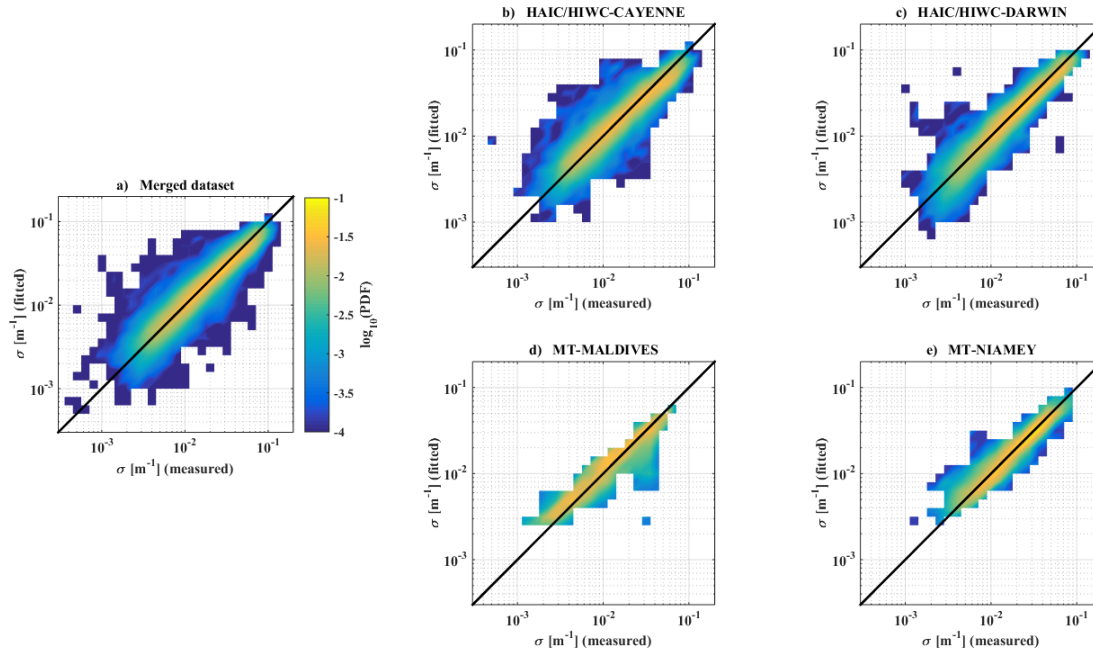


Figure R2: Visible extinction calculated from equation (8) on y-axis as a function of measured visible extinction on x-axis. a) for the merged dataset, b) for the Cayenne campaign, c) for the Darwin campaign, d) for the Maldives campaign and e) for the campaign over Niamey. Probability distribution function (PDF) are given by the color scale. Black line represent the function $x=y$.

Figure R2 show that visible extinction computed with equation (3; in the original versions of the manuscript) versus measured visible extinction are mainly distributed around the black curve $y=x$.

Some change have been made for the section concerning the parameterization of visible extinction (R2#12).

“6.1 visible extinction

Since we concluded from Figure 7 and Figure 8 that visible extinction σ and IWC in tropical MCS tend to be similar for all MCS locations in the same range of T and for corresponding MCS reflectivity zones 4 to 8. Moreover Figure 19 shows that there is a linear relationship between $\log(\sigma)$ and $\log(IWC)$. And $\log(\sigma)$ decrease with temperature increasing at constant $\log(IWC)$. Then, we performed a surface fitting using input coefficients $\log(IWC)$ and T to fit $\log(\sigma)$ to deduce a parametrization of σ (Eq. (8)) as a function of IWC and T for deep convective cloud data (merged dataset) of this study limiting data to $IWC > 0.1g m^{-3}$:

$$\sigma = \exp(-0.0194587 \cdot T + 0.9134019 \cdot \ln(IWC) + 1.2423609) \quad [m^{-1}] \quad (8)$$

page 12, line 22: “... identical image data processing to remove shattering artefacts...”
 which method exactly do you use? This might be quite important for the resulting data.
 For example, when you use the interarrival time method from Field et al., 2006, using the same time threshold for all data sets might lead to errors. The best threshold might even vary from one flight to the next in the same campaign (at least in my experience, see e.g. Frey et al., 2011, where interarrival times have been adapted for each single flight). Thus, using only one threshold for all four campaigns might lead to removal of ‘good’ images in one case and incomplete removal of ‘bad’ images in another case.

As it is not the first publication using part of this dataset, and that processing applied to this is exactly the same as in Leroy et al. (2016 and 2017) we give the reference if the reader wants more details; in the manuscript page 3 line 34:

“Accurate description of data processing is documented in Leroy et al. (2016 and 2017), Protat et al. (2016), Strapp et al. (2016b), and Davison et al. (2016).”

Indeed, Field et al., (2006) was used to remove shattering. Except, that the cut off time threshold computed using Gaussian function to fit inter-arrival time of natural particle and Gaussian function to fit inter-arrival time of shattered particles, were calculated every second; both for PIP and 2D-S probe.

More details in Leroy et al., (2016): “In addition, a fraction of cloud particles inevitably hit the probe’s housing during sampling and may break up into multiple fragments that are recorded by the probe (Field et al. 2003; Korolev and Isaac 2005; Heymsfield 2007). During the HAIC/HIIWC field campaign, the frequency of such events was reduced by using specially designed probe leading edge tips to minimize shattering. However, the remaining images related to splashing/shattering events had to be removed as effectively as possible; otherwise, PSD measurements and their derived microphysical properties would be subject to errors. Most of the images related to a shattering/splashing event were removed by a careful analysis of (i) the ratio between the particle’s area and its sizes in the x and y directions and (ii) the interarrival times between neighboring particles. The interarrival time technique is commonly used and has been described and tested by Field et al. (2006), Baker et al. (2009), Lawson (2011), and Korolev and Field (2015). In this study, the image processing rejected particles presumed to be associated with shattering if their interarrival times were lower than a cutoff value that was calculated once per second.”!

page 12/13, Section 5.3 until page 13, line 20: Since the conclusions from Figure 8 and 9 are similar, and due to the uncertainties related to the small particles, I think Fig. 8 and the corresponding text would be a good candidate to move to a supplement and only briefly mention here. See main comment about the length of the manuscript above.

We agree, and put figure 8 (in the old manuscript) on total concentration in the appendices A (R2#13).
“

Appendices A

Figure A1 shows median total concentration (N_T) as a function of T and MCS reflectivity zone (N_T) for the merged datasets where concentrations of ice hydrometeors are integrating beyond $15\mu\text{m}$:

$$N_T = \sum_{D_{max}=15}^{D_{max}=12845} N(D_{max}) \cdot \Delta D_{max} \quad [L^{-1}] \quad (A1)$$

Median N_T systematically increase with MCS reflectivity zone and altitude, however with significant overlap of 25th and 75th percentiles of neighboring MCS reflectivity zones. Measurement uncertainty on concentrations given for small hydrometeors is about $\pm 100\%$ (Baumgardner et al., 2017).

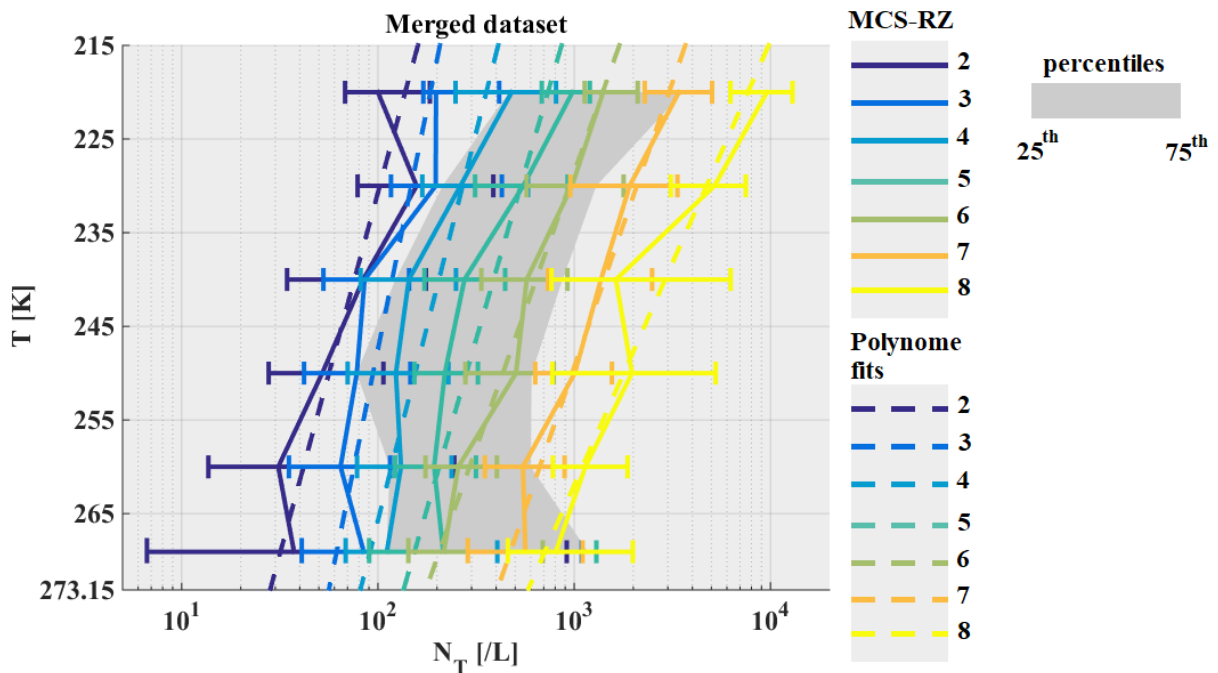


Figure A1: Same as Figure 5, but for concentrations of hydrometeors integrated beyond $D_{max} = 15\mu\text{m}$ in $[L^{-1}]$.

Figure A2 (a), Figure A2 (b), Figure A2 (c), and Figure A2 (d) show MRD- N_T of MCS in the different tropical locations. For MCS over Darwin and Cayenne, in all MCS reflectivity zones MRD- N_T are smaller than the measurement uncertainty, whereas for Niamey data this is the case only in MCS reflectivity zones 2, 5, 6 and 7. MCS over Maldives Islands yield significantly larger MRD- N_T than the measurement uncertainty, and those are primarily positive. Hence, MCS over Maldives Islands have larger concentrations of hydrometeors for a same range of T and Z, than the three other types of tropical MCS. However, these larger concentrations observed do not concern zones where highest concentrations of hydrometeors were observed. For example, in MCS reflectivity zone 4 where MRD- N_T is reaching 1000%, N_T for the Maldives dataset are approximately $1000 L^{-1}$, which is similar to N_T observed in MCS reflectivity zones 7 and 8 for the same range of $T \in [235K; 245K]$ for the merged dataset. We recall that identical image data processing to remove shattering artefacts and to correct for out of focus images (Field et al., 2003; Korolev and Isaac, 2005; Leroy et al., 2016) have been applied for all 4 tropical datasets. Also the presence of super cooled droplets has been investigated (RICE, CDP probe), and few periods with super cooled water content have been removed for this study. Moreover, we show in section 5.5 that MCSs over Maldives Islands tend to have smaller $\max(D_{max})$ especially in MCS reflectivity zones 4, 5, 6 and 7 compared to the other MCS locations and that concentrations beyond $500\mu m$ in Maldives Islands observations are in the same range as the other types of MCS.

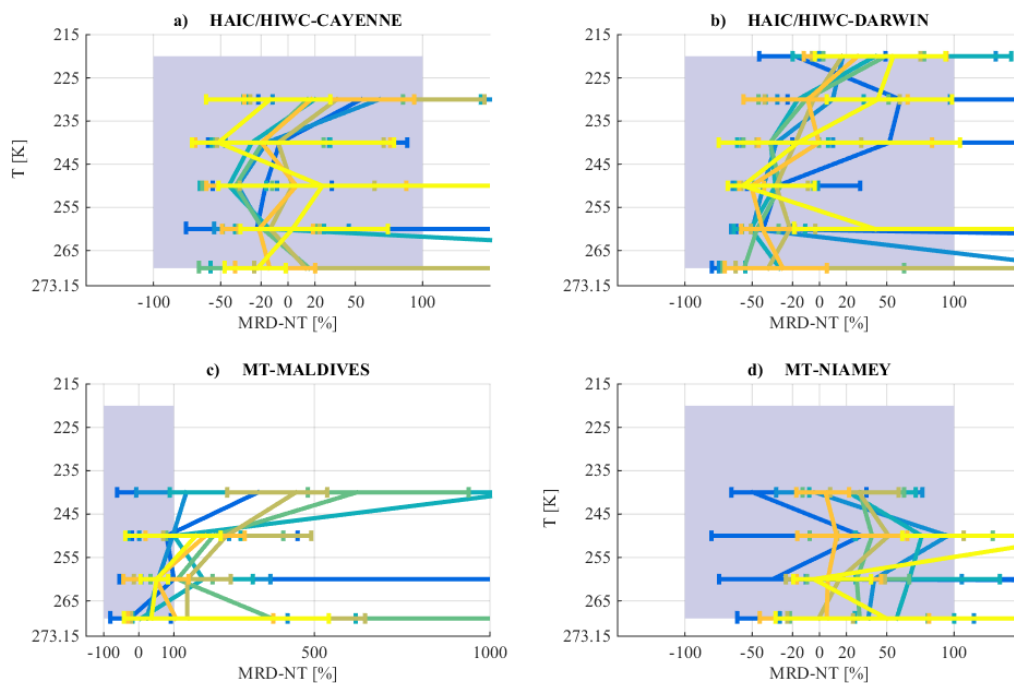


Figure A2: Same as Figure 6, but for MRD-NT.

”

page 14, line 30: “in the decaying parts”

I think here is the first time where you mention these MCS to be decaying. Is it true for the whole of the Maldives measurements, or only for parts of the measurements with the small particles (or only for specific Z)? This relates to my main comment about the meteorological differences between the MCSs in the different campaigns.

No this is a misunderstanding we are talking about the decaying part of MCS, contrary to the active part of the MCS (convective area).

We propose to rephrase this sentence (R2#14):

“We observe that total concentrations starting from $15\mu m$ can be different between MCS locations as a function of T and Z, especially in oceanic MCS over Maldives Islands in the more stratiform part of these MCSs where measured concentrations can reach 10 times the median concentrations observed globally for merged tropical dataset.”

page 15, line 29/30: What are ep and es?

They are respectively the pre-factor of the perimeter-size relationship and the pre-factor of the surface-size relationship; power-law relationship. However, they have no interest in our study. They are here, to write correctly the equations.

page 16, line 10: “merged with subsequently sampled rather small local convective systems”

Since you focus your study on MCS, can these rather small convective systems still be classified as MCS? Otherwise, should they not be removed from the data set?

MCS over Maldives in the second period of the campaigns were weaker because of the dry phase of the MJO. However, the dataset over Maldives is quiet small (compared to others) and these data are still related to convective systems. So we decided to keep these data.

But this part has been rewritten and this the discussion linked to this comment deleted. Has we are no longer agree that it is due to a lack of statistic (it would be the same for all parameters). We simply agree that shape of hydrometeors are different in these condition for the Maldives (see new section 5, in the major comment section).

page 15-17/Section 5.4:

Maybe this section could also go into the supplement (no major conclusion drawn)? and only briefly mention in main manuscript.

This section study the shape of ice hydrometeors (β) coefficient and somewhere their density (α). Tendencies and results given in this section might interest scientist community working on mass-size relationship. We keep it, but some change have been made (see new section 5 in the major comment section).

page 17/18, section 5.5:

Also this section could be moved to a supplement?

Length of section 5 have been reduced, we want this part stay in the main part of the manuscript. As the section 5.4 before, it shows that ice hydrometeors can be different in some of their properties. Even if they are similar considering their IWC or visible extinction.

page 18, line 22: “Commonly, number PSD of ice hydrometeors are modeled with Gamma distributions.”

Maybe give one or two example references.

We propose to add these two references (R2#15):

Heymsfield, A. J., Schmitt, C. and Bansemer, A.: Ice Cloud Particle Size Distributions and Pressure-Dependent Terminal Velocities from In Situ Observations at Temperatures from 0° to -86°C, *J. Atmos. Sci.*, 70(12), 4123–4154, doi:[10.1175/JAS-D-12-0124.1](https://doi.org/10.1175/JAS-D-12-0124.1), 2013.

McFarquhar, G. M., Timlin, M. S., Rauber, R. M., Jewett, B. F., Grim, J. A. and Jorgensen, D. P.: Vertical Variability of Cloud Hydrometeors in the Stratiform Region of Mesoscale Convective Systems and Bow Echoes, *Monthly Weather Review*, 135(10), 3405–3428, doi:[10.1175/MWR3444.1](https://doi.org/10.1175/MWR3444.1), 2007.

page 22, line 22: How would M3 derived from parameterised M2 according to Eq. (18+13) look lie? Why don’t you show this as well? Above you make an improvement to theM2 parameterisation, so why do you use the presumably worse parameterisation for deriving M3 here now? Which would also presumably lead to a worse M3 retrieval?

This part is modified, to make it easier to understand. Relative errors are plotted separately for the 2nd moment and for the third moment. There, is no change for the 2nd Moment except that a new function (18; now 17) has been calculated for IWC in [kg.m⁻³] (NWP units).

Then, we show only the relative error for M3 derived with M2 using equation (14; now 13); the original parameterization of Field et al., (2007). As for equation (18; now 17) we computed a new equation (19; now 18) where IWP is in [kg.m⁻³].

In this new version of manuscript, we show relative error for three other computation of the third moment. First, when the equation (19; now 18) is applied with measured M2, to show efficiency of the equation (19; now 18). Then, when the equation (19; now 18) is applied to M2 derived from the equation (12; now11) when there is no correction for the calculation of M2 as function of IWC. It show that equation (19; now 18) fails to compute M3 for large IWC if M2 are not calculated correctly with equation (18; now 17). Finally, when the equation (19; now 18) is used with M2 calculated with equation (18; now 17), it show the efficiency of the new parameterization of M2 and M3 developed in our study.

The new version is written after the new section 5 (in section 6.2.2) in the major comment section.

page 23, line 14/15: “blue solid lines represent median relative error when estimated

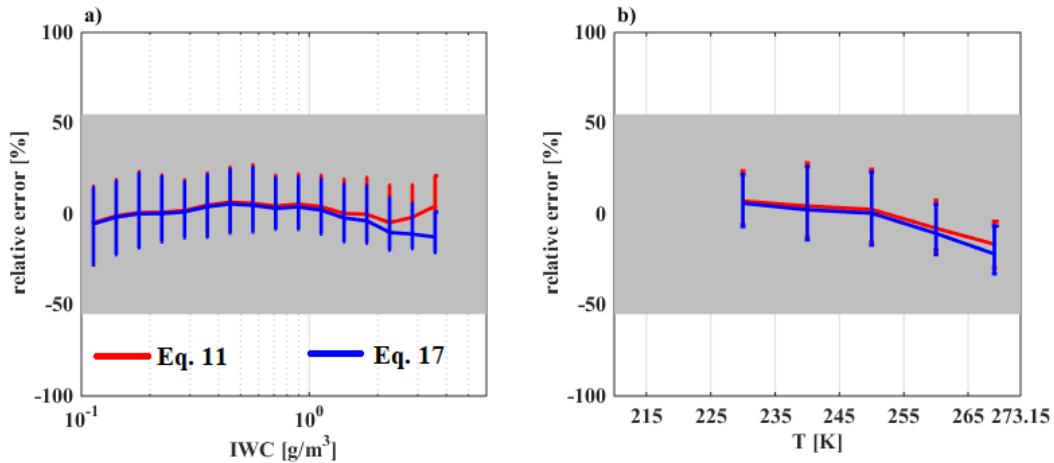
M3 is calculated from parametrized M2 from Eq. (18+13) and Eq. (19).”
 This is not, what the legend in Figure 17 says?
 See new version, this has been changed.

page 23, lines 19-27: Maybe show the figures in a supplement?

We agree to show the figures in the reviewer answer. However, the new version of the manuscript has already a lot of figures and 3 more Appendices.

HAIC-HIWC Cayenne

Median relative error for parameterizations of second Moment of PSD



Median relative error for parameterizations of third Moment of PSD

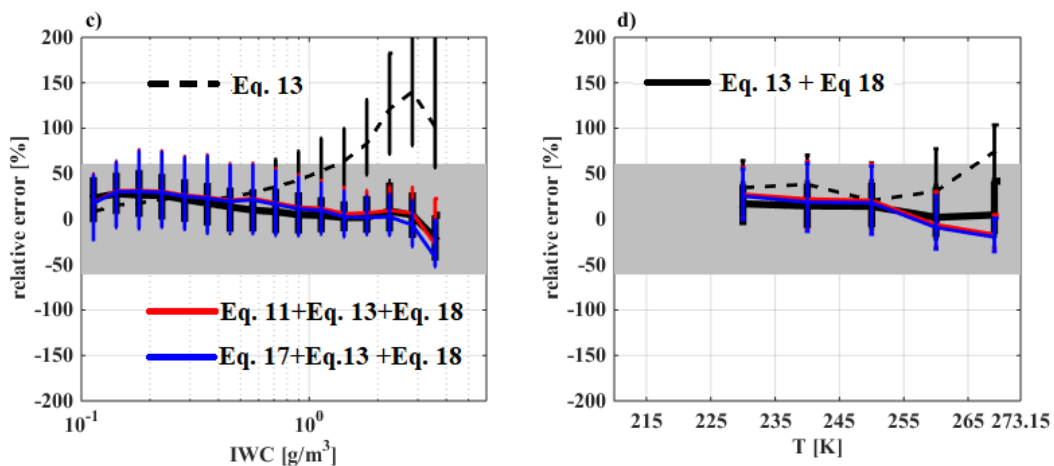
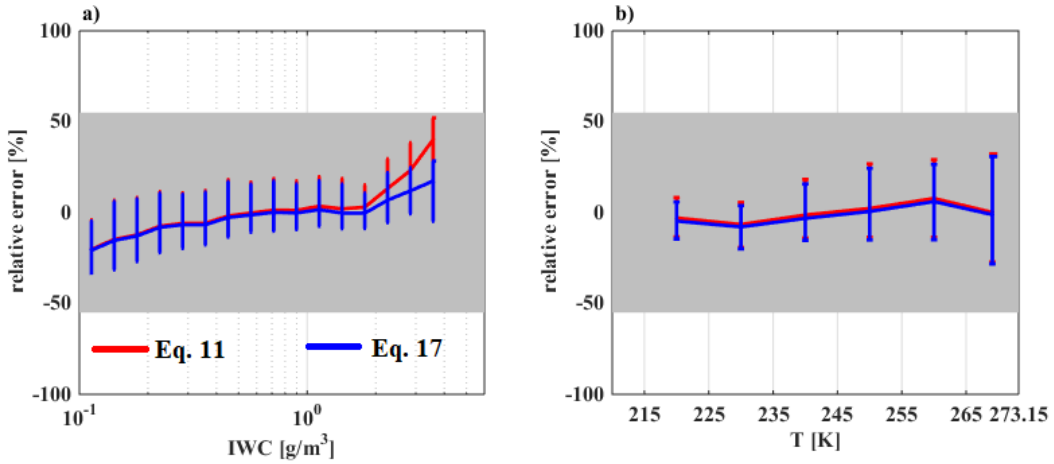


Figure R 3: Relative error of parametrized M_2 and M_3 for MCS over Cayenne as a function of IWC in a) and c), and as a function of T in b) and d). Solid lines give median relative error and whiskers denote 25th and 75th percentiles of relative error. Grey bands shows measurement uncertainties for M_2 (55%; a) and b)) and M_3 (61%; c) and d)), respectively

HAIC-HIWC Darwin

Median relative error for parameterizations of second Moment of PSD



Median relative error for parameterizations of third Moment of PSD

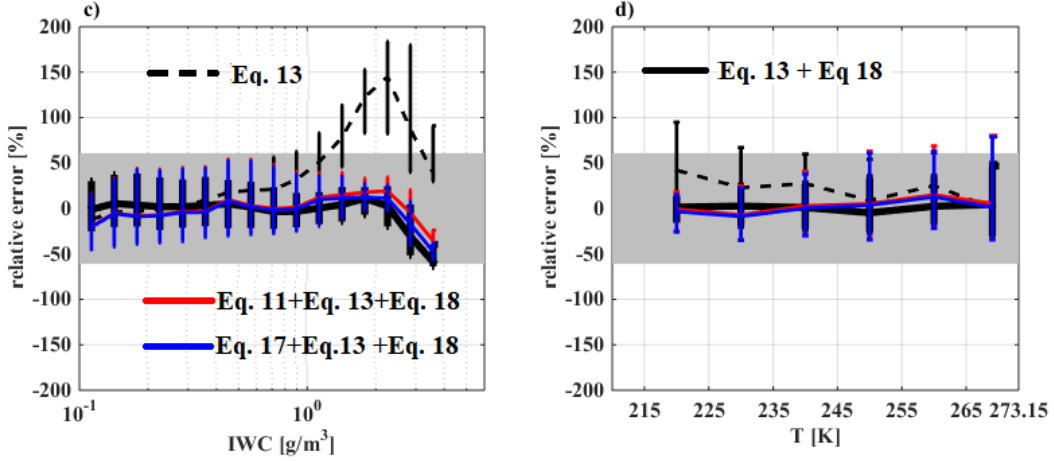
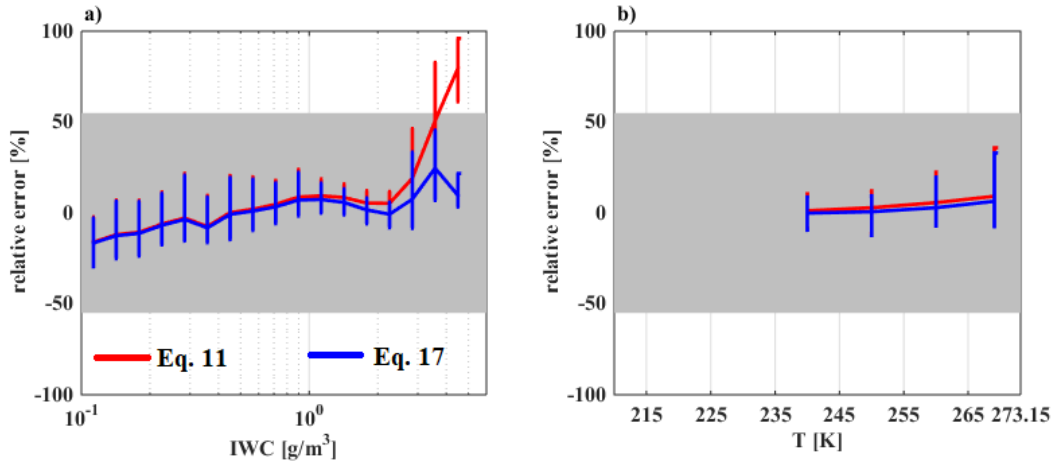


Figure R4: Relative error of parametrized M_2 and M_3 for MCS over Darwin as a function of IWC in a) and c), and as a function of T in b) and d). Solid lines give median relative error and whiskers denote 25th and 75th percentiles of relative error. Grey bands shows measurement uncertainties for M_2 (55%; a) and b)) and M_3 (61%; c) and d)), respectively

MT-Niamey

Median relative error for parameterizations of second Moment of PSD



Median relative error for parameterizations of third Moment of PSD

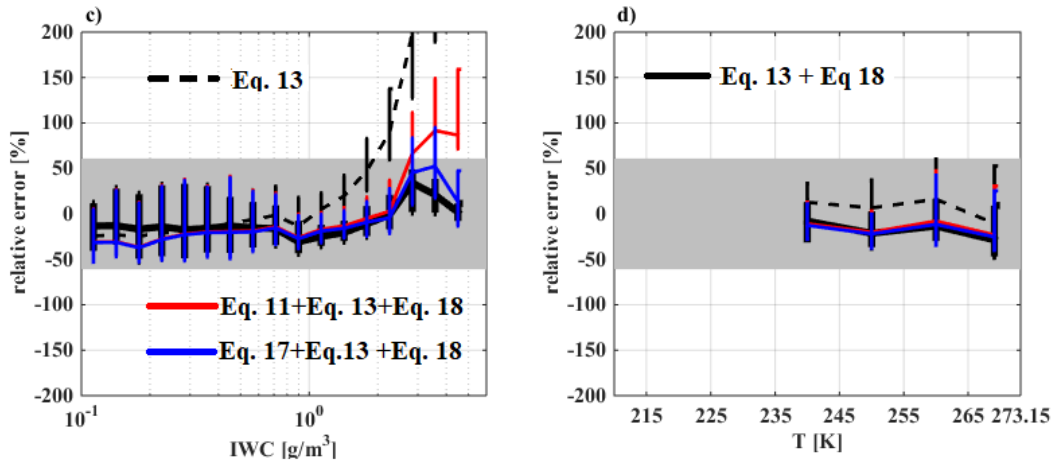
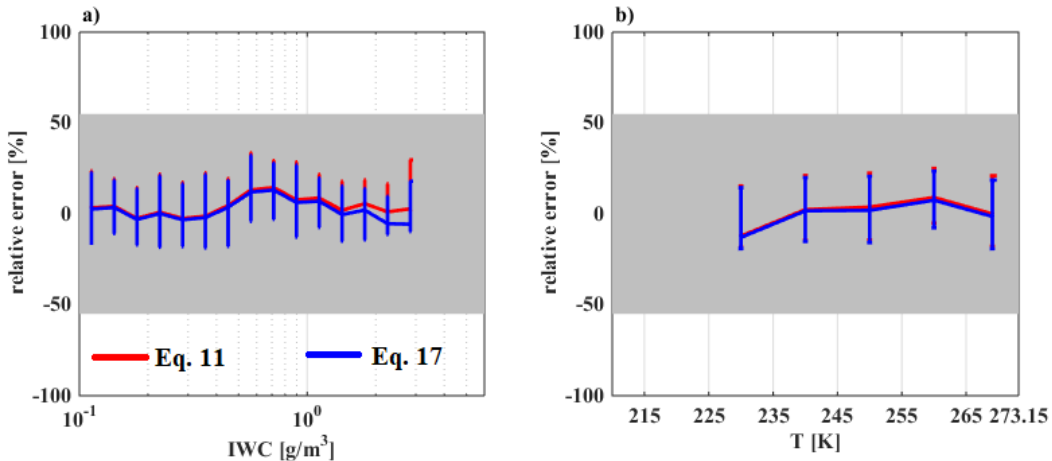


Figure R5: Relative error of parametrized M_2 and M_3 for MCS over Niamey as a function of IWC in a) and c), and as a function of T in b) and d). Solid lines give median relative error and whiskers denote 25th and 75th percentiles of relative error. Grey bands shows measurement uncertainties for M_2 (55%; a) and b)) and M_3 (61%; c) and d)), respectively

MT-Maldives

Median relative error for parameterizations of second Moment of PSD



Median relative error for parameterizations of third Moment of PSD

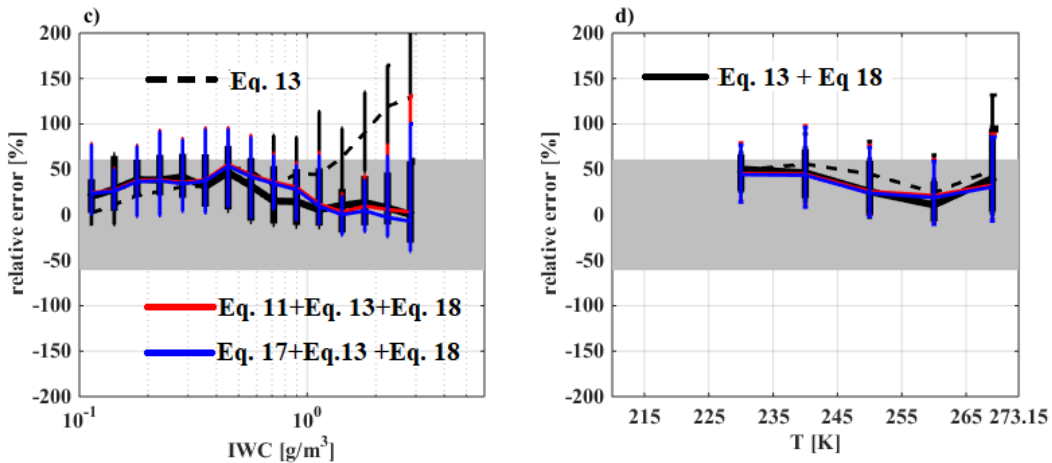


Figure R6: Relative error of parametrized M_2 and M_3 for MCS over Maldives as a function of IWC in a) and c), and as a function of T in b) and d). Solid lines give median relative error and whiskers denote 25th and 75th percentiles of relative error. Grey bands shows measurement uncertainties for M_2 (55%; a) and b)) and M_3 (61%; c) and d)), respectively

page 24, line 20: “extrapolates PSD” - I think you mean measured PSD (I strongly suggest to never extrapolate any PSD!). Please rephrase!

This sentence need more informations (R2#16)

“, whilst this study extrapolates PSD until 1.2845cm only (reconstruction of partial images to calculate particle size according to Korolev and Sussman 2000).”

page 25, line 32/33: Is there a difference between zones 1-5 or would it actually suffice to combine them into one reflectivity zone? (related to my main comment on radar reflectivity zones)

It seems that there is no difference in dynamic, they have all low probabilities of vertical movement. Then, low probabilities to be associated with convective zones. That is why we assume they are all more related to the stratiform part of MCS. However, they have different range of IWC, Z , total concentrations, and visible extinction. Moreover, there is no confident measurement of IWC in MCS reflectivity zone 2 and 3. So, we prefer to give our results as they are with the 8 MCS zones. And future investigations could improve our view of the difference in each MCS reflectivity zones.

page 26, lines 14-20: Would it be possible to make a more general point here: Possibly that aggregation process efficiency is higher for convection over land than over islands and higher over islands close to large land masses than over islands in the middle of an ocean? Are there other studies you could relate to? Or is it the convective system size (larger in Niamey...)?

Unfortunately, the impact of the size of MCS has not been investigated yet.
(R2#17)

“aggregation process efficiency is higher for convection over land than over islands and higher over islands close to large land masses than over islands in the middle of an ocean. It seems to confirm the results of Frey et al., (2011) and Cetrone and Houze (2009).”

Technical corrections

page 2, line 34: “predictions fails” - predictions fail

page 3, line 18: an 'and' missing: “..., and the cloud radar RASTA...”

page 4, line 14: Should be 4, not 5 airborne campaigns.

**page 7, line 11, and page 8 line1: “(Figures 5, 6, 8, 9, 10, 11, 12, 13, 14, 15 and 16)”
better (Figures 5, 6, and 8 - 16)**

page 8, line 17: “Globally”- do you mean 'generally'?

page 10, line 14: start with lower case 'with' after equation.

page 18, line 15: “different from one MCS type of MCS to another” remove 'of MCS'.

**page 26, line 5: “for individual the MCS locations),”
remove 'the' and ')'.7**

Figures and Tables

Figure 1: This plot is very busy. Maybe it would be easier to read if you split the figure into four subfigures (one for each campaign) with the black lines for the merged data set in each of the subfigures?

We think it is necessary and more interesting to see all the percentiles profiles of the merged dataset and the four campaigns. It allows to compares them to each other's. Also the goal of this figure is to show the limit of the MCS reflectivity zones.

Figure 2: Colours: Generally, it is advised to choose colourblind-friendly colour schemes, and the rainbow scheme is unfortunately not one of those (among other shortcomings of this colour table, see e.g. the open letter to the scientific community here: <https://www.climate-lab-book.ac.uk/2014/end-of-the-rainbow/>). In subfigure b, I find it hard to distinguish between MCS zone 2 and 3, thus a different colouring would help here, too.

The axis labels (numbers) are too small, please enlarge.

Done, see new figures in the new section 5 and 6, in the answer of the major comment concerning length of section 5.

Figures 5, 6, and 8 - 16:

I don't think it is important to name the campaigns each time, it suffices to mention the locations (also in figure captions and text).

The subfigures are rather small, maybe you could move the legends to the top or bottom of the figure to allow more space for the subfigures?

Done, see new figures in the new section 5 and 6, in the answer of the major comment concerning length of section 5.

Caption line 1/2: Maybe better: ... for the different MCS reflectivity zones using the results from the four locations. (removing the second sentence)

I cannot see to where this comment is related to.

Figure 7: You say IWC in the caption but the figure label say CWC. Same in Figure 17.
Correction done.

Figure 14: The caption says “for M2 per for unity dimension.”, the axis annotation says: “M2 [m-1], so not unity dimension. Please clarify.

The true unit is [m⁻¹]. Correction done

Figure 18: See comment about colours above.

A new figure with colourblind-friendly colours is made.

Table 2: The table is extremely hard to read, unfortunately! Maybe it could help to swap the 'with respect to median of' column with a 'radar reflectivity zone' column, and give the parameters in front of the temperature brackets.

Indeed, the table is complex to read. We do not understand the suggestion as there is no column "with respect to median of". However we suggest to shift this table in a last Appendices.

Tables in Appendix: I assume that the decimal point should actually be a point and not a comma - as in all your appendix tables?

Corrections done.

References

Field, P. R., Heymsfield, A. J., and A. Bansemmer: Shattering and Particle Interarrival Times Measured by Optical Array Probes in Ice Clouds, Journal of Atmospheric and Oceanic Technology, 23, 1357-1371, 2006

Frey et al.: In situ measurements of tropical cloud properties in the West African Monsoon: upper tropospheric ice clouds, Mesoscale Convective System outflow, and subvisual cirrus, Atmos. Chem. Phys., 11, 5569-5590, 2011